CHALMERS

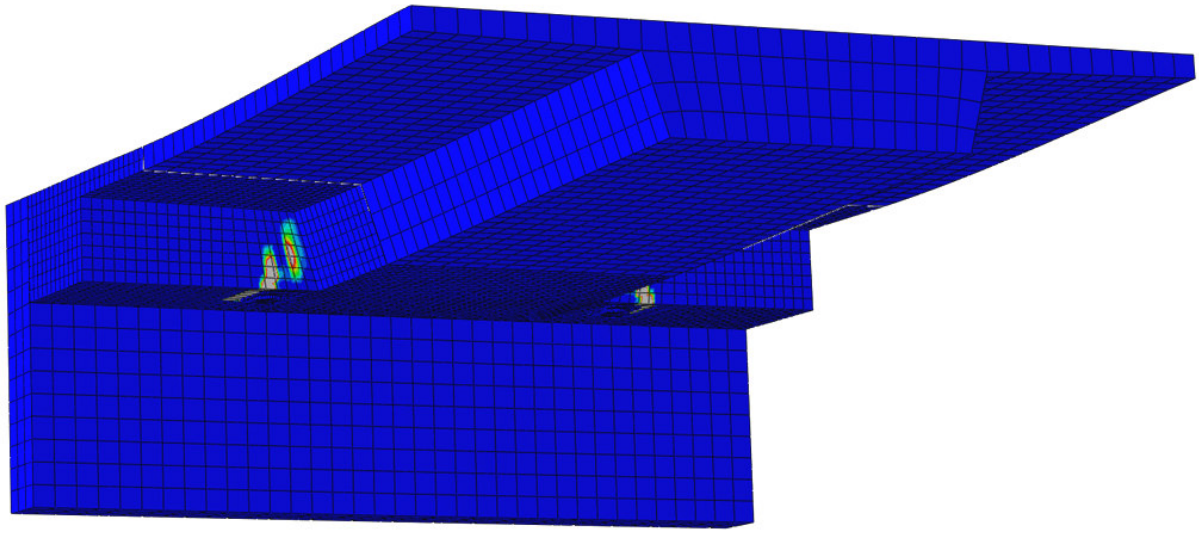

FE-analysis of cracking in transversal support beams of concrete bridges

Investigation into the cause of detected cracks

Master of Science Thesis in the Master's Program Structural Engineering and Building Performance Design

MAX FREDRIKSSON

HÅKAN YHLEN

Department of Civil and Environmental Engineering
Division of Structural Engineering
Concrete structures
CHALMERS UNIVERSITY OF TECHNOLOGY
Göteborg, Sweden 2010

Master's Thesis 2010:6

MASTER'S THESIS 2010:6

FE-analysis of cracking in transversal support beams of concrete bridges

Investigation into the cause of detected cracks

Master of Science Thesis in the Master's Program Structural Engineering and Building Performance Design

MAX FREDRIKSSON

HÅKAN YHLEN

Department of Civil and Environmental Engineering
Division of Structural Engineering
Concrete structures
CHALMERS UNIVERSITY OF TECHNOLOGY
Göteborg, Sweden 2010

FE-analysis of cracking in transversal support beams of concrete bridges
Investigation into the cause of detected cracks

Master of Science Thesis in the Master's Program Structural Engineering and Building Performance Design

MAX FREDRIKSSON

HÅKAN YHLEN

Examensarbete / Institutionen för bygg- och miljöteknik,
Chalmers tekniska högskola 2010:6

Department of Civil and Environmental Engineering
Division of Structural Engineering
Concrete structures
Chalmers University of Technology
SE-412 96 Göteborg
Sweden
Telephone: + 46 (0)31-772 1000

Cover:
FE-model of bridge at road junction Axevalla, 16-935-1, showing the obtained crack pattern at the transversal support beam when self-weight and prestress is applied.

Chalmers Reproservice
Göteborg, Sweden 2010

FE-analysis of cracking in transversal support beams of concrete bridges
Investigation into the cause of detected cracks

Master of Science Thesis in the Master's Program Structural Engineering and Building Performance Design

MAX FREDRIKSSON

HÅKAN YHLEN

Department of Civil and Environmental Engineering
Division of Structural Engineering
Concrete structures
Chalmers University of Technology

ABSTRACT

Cracking has been detected in transversal support beams in a number of concrete bridges in Sweden during the last few years. The reason for these cracks has been unknown until today, and a more detailed study of the problem has been asked for. This report includes an inventory of existing bridges that have experienced cracking in their transversal support beams. The inventory showed that cracking has occurred in several post-tensioned bridges in Vägverket's Region West during the last years. The bridge at road junction Axevalla, 16-935-1, was chosen for a case study. In the case study, the finite element software BRIGADE/Plus was used to simulate the cracking behaviour using non-linear material models for concrete. The result of the case study showed that the prestressing force alone caused the cracks, while vertical loads have not affected the cracking. The prestressing force causes shortening of the main beam and, since the cantilevering parts of the bridge slab is not equally compressed, bending of the transversal beam in the horizontal plane. Since the other bridges included in the inventory are of similar design it is likely that also these bridges have cracked due to the prestressing force. A parametric study has been performed to find which measures that can be taken in the future to limit cracking in similar bridges. The parametric study involved widening of the transversal beam, inserting wedges in the corners between the transversal beam and the main beam, changing the boundary conditions of the transversal beam and adding more reinforcement in the transversal beam. The results from the parametric study showed that the most efficient way to limit the cracks in length and width was to insert more horizontal reinforcement in the front face of the transversal beam.

Key words: Concrete bridges, cracks, cracking, non-linear FEM, transversal beam, prestress, post-tensioned

FE-analys av sprickbildning i ändtvärbalkar i betongbroar

Undersökning av orsaken till befintliga sprickor

Examensarbete inom Structural Engineering and Building Performance Design

MAX FREDRIKSSON & HÅKAN YHLEN

Institutionen för bygg- och miljöteknik

Avdelningen för konstruktionsteknik

Betongbyggnad

Chalmers tekniska högskola

SAMMANFATTNING

Sprickbildning har upptäckts i ändtvärbalkarna på ett antal betongbroar i Sverige under de senaste åren. Anledningen till dessa sprickor har varit oklar fram till i dag, och en mer detaljerad studie av problemet har efterfrågats. En inventering av befintliga broar som har haft problem med sprickbildning i ändtvärbalkar har gjorts. Inventeringen visade att sprickbildning har förekommit i flera efterspända broar i Vägverkets Region Väst under de senaste åren. Bron över väg 49 vid trafikplats Axevalla, 16-935-1, valdes för en fallstudie. I fallstudien användes finita element programvaran BRIGADE/Plus för att studera sprickbildningen. Med hjälp av icke-linjära materialmodeller för betong kunde sprickorna påvisas i FE-modellen. Resultatet av fallstudien visade att endast förspänningskraften har orsakat sprickorna, medan vertikala laster inte har påverkat sprickbildningen. Spännkraften leder till att brons huvudbalk trycks ihop och, eftersom de utkragande delarna av brobaneplattan inte trycks ihop lika mycket, till att ändtvärbalken böjs i horisontalplanet. Då de andra broarna som omfattats av inventeringen har liknande utformning är det troligt att även sprickbildningen i dessa har uppkommit på grund av förspänningskraften. En parameterstudie har genomförts för att se vilka åtgärder som kan vidtas för att i framtiden begränsa sprickbildningen i liknande broar. I parameterstudien testades att bredda ändtvärbalken, att lägga in voter i korsningen mellan huvudbalk och ändtvärbalk, att tillåta fri rörelse i tvärled för ändtvärbalken samt att lägga in mer armering i framsidan av ändtvärbalken. Parameterstudien visade att det mest effektiva sättet att begränsa sprickornas utbredning och storlek var att lägga in mer armering i framsidan av ändtvärbalken.

Nyckelord: Betongbroar, sprickor, sprickbildning, icke-linjär FEM, ändtvärbalk, förspänning

Contents

Preface

This master thesis concludes the authors' Masters of Science Degree in Civil Engineering, specializing in Structural Engineering, at Chalmers University of Technology. The report and analyses has been conducted at Inhouse Tech´s office in Göteborg between October 2009 and April 2010.

We would like to thank our examiner Ph.D. Mario Plos at the Department of Civil and Environmental Engineering, Concrete Structures, Chalmers University of Technology, Sweden and our supervisor Rikard Migell at Inhouse Tech for assistance and guidance during the work.

We would also like to thank all people that provided us with structural drawings and information related to this project. For guidance performing the FE-analyses we would like to express our appreciation to the people at Scanscot Technology, Lund, Sweden.

To our opposition group, Patrik Eriksson and Emanuel Trollin, we would like to thank for constructive criticism through the project.

Finally we would like to thank the people on the second floor of Magasinsgatan 22 for good advises and entertainment during the coffee breaks.

Göteborg April 2010

Max Fredriksson

Håkan Yhlen

Notations

Roman upper case letters

A_t	Cross-sectional concrete area of main beam
A_t	Cross-sectional area of tendon
C_1, C_2	Material constants for concrete
E	Young's modulus
E_{cm}	Young's modulus of concrete, mean value
G_F	Fracture energy
I_b	Moment of inertia for main beam
I_{tb}	Moment of inertia for transversal beam
K_c	Factor that changes the yield surface in the deviatoric plane
L	Length
M	Moment
M_0	Bending moment in field
P_i	Force in tendon
P_{ini}	Initial prestressing force
R	Reaction force
S	Statical moment of area
T_1, T_2	Reaction force at bearings, transversal direction
V_0	Shear force at support
V_1, V_2	Reaction force at bearings, vertical direction

Roman lower case letters

$f_{ctk0,05}$	Tensile strength of concrete, 5^{th} percentile value
f_{cm}	Concrete compressive strength, mean value
f_{st}	Yield strength of steel
g	Gravity constant
h	Height
k	Angular displacement
l_{mb}	Width of main beam
q	Distributed load
s	Length of tendon from active end to section under consideration
t	Thickness
z	Distance in vertical direction

z_{GC} Distance vertical direction from bottom of member to centre of gravity

u_1, u_2, u_3 Translational degrees of freedom

u_4, u_5, u_6 Rotational degrees of freedom

w Width of crack

w_u Ultimate crack opening

Greek letters

α Change of slope over a certain distance

α_e Expansion coefficient

α_E Slope of concrete stress-strain curve for elastic strain

ε Eccentricity

ε_{cc} Concrete compressive strain

ε_{cc1} Concrete compressive strain when $\sigma_{cc} = f_{cm}$

ε_{cu1} Concrete nominal ultimate strain

ε_{pl} Plastic strain

$\varepsilon_{pl,t}$ Tensile equivalent plastic strain

μ Viscosity parameter

μ_f Frictional parameter

ν Poisson's ratio

ρ Density

σ Stress

σ_1 Maximum principal stress

σ_{B0} Initial equibiaxial compressive yield stress

σ_{C0} Initial uniaxial compressive yield stress

σ_{cc} Concrete compressive stress

σ_{le} Stress at lower edge

σ_t Stress in tendon

σ_z Normal stress in vertical direction

ϕ Diameter of reinforcement

ψ Dilation angle

1 Introduction

1.1 Background

Some concrete beam bridges, with load-carrying transversal beams over supports, have recently experienced quite extensive cracking in the transversal beams, as shown in Figure 1.1. As for all cracks in concrete these cracks are strongly related to the durability of the structure, for example problem with reinforcement corrosion due to intrusion of chlorides or early carbonation of the concrete. The Swedish road administration, Vägverket, have taken some actions to handle this problem. Vägverket have in their design code, Bro 2004 – Supplement nr, section 42.212, harshened the demand for suspension reinforcement in the transversal beam. The primarily effect of this change is that the shear force reinforcement can no longer be included as part of the suspension reinforcement in this region. Recommendations have also been given to avoid sharp inward-bound corners and abrupt changes of cross-section near the transversal beam. The recommendation is then to instead make the change of cross-section smoother by adding a wedge in the transition between the main beam and the transversal beam according to Vägverket (2005). However, these actions have not been fully successful and there is a need of better understanding of the problem and another design solution would be preferable.

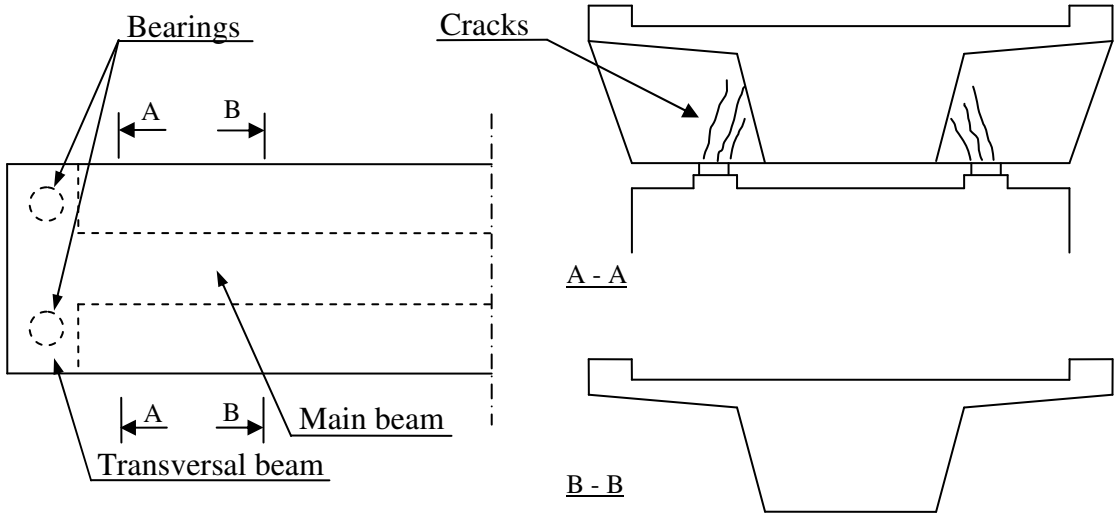

Figure 1.1 Sketch of the bridge type studied in the master's thesis, and location of cracked regions.

1.2 Purpose

The purpose of the master's thesis is to investigate the circumstances around cracking of transversal support beams in concrete bridges and to identify the reason of these cracks. The aim is also to examine how different changes in the design of the transversal support beam influence the result in terms of tensile stresses and cracking of the transversal beam.

1.3 Objectives

A number of objectives should be fulfilled in order to realize the purpose of the thesis. These correspond to the main parts of the project and are in principle the following:

- Study documentation from existing bridges which have experienced cracking in transversal support beams in order to identify design procedures and structural layouts that are common for these bridges.
- Perform an analysis of one certain selected bridge with the finite element, FE, software BRIGADE/Plus to see if cracking can be detected in a non-linear analysis.
- Develop the finite element model by introducing changes to the design, and to study the effect of these changes in order to find recommendations for future bridges.

1.4 Scope

The scope of this master's thesis concerns concrete road bridges in Sweden, of the type illustrated in Figure 1.1. The bridge type of interest is single beam bridges with load-carrying transversal beams over the end supports. Both prestressed and non prestressed bridges are of interest.

The thesis treats cracks starting in the region directly above the bearings, propagating straight or slightly inclined upwards towards the main beam, as illustrated in Figure 1.1.

1.5 Method

The inventory of existing bridges with the design and crack pattern of interest has been made by searching the database Batman. Batman is Vägverket's database of existing bridge and tunnel structures which contains technical information, drawings and remarks from inspections. Certain selected bridges have then been chosen to be investigated more in detail. Additional information, such as crack mappings and design calculations, has then been gathered from sources such as Vägverket's archive and companies and persons involved in the respective projects.

The FE-software used in the project was BRIGADE/Plus 3.1-1. BRIGADE/Plus is developed primarily for design and analysis of bridges and is based on the more general FE-software Abaqus.

The FE-analyses were verified both by comparison to hand calculations and to analyses made in STRIP STEP2 version PC-02. STRIP STEP2 is a text-based program for calculations of frame and truss structures, and has been used for bridge design in Sweden to a large extent since it was developed in the late 1960's. The extensive use of the program during long time has contributed to the good reputation that the program have today.

2 Inventory of damaged bridges

This section treats bridges where damage in form of cracks has been discovered on transversal support beams. The choice of the bridges studied has been based on the bridge type and the crack pattern that has been detected during inspections. The bridge type that has been of interest is concrete bridges with one longitudinal main girder with transversal support beams at the end supports. Both prestressed and non-prestressed bridges have been of interest, but only prestressed bridges were found with the crack pattern of interest. Cracks which have been of interest in this inventory are vertical or slightly inclined cracks on the front face of the transversal beams, in the regions above the bearings, as indicated in Figure 1.1. Only bridges located in Vägverket's Region West has been included in the inventory. A few other bridges than the ones presented below have been found with similar crack patterns; they are however not presented in this chapter due to lack of documentation from these cases.

2.1 Bridge at road junction Axevalla, 16-935-1

Bridge 16-935-1, located at junction Axevalla between Skara and Axvall over road 49 was built during year 2009 by the contractor PEAB. The bridge was designed by FB Engineering AB and is a post tensioned concrete bridge.

The bridge consists of three spans with lengths of 21 m + 34 m + 21 m = 76 m. The transversal support beams are located over support 1 and 4, see Figure 2.1 for elevation of the bridge and Figure 2.2 for the detail of the transversal beam. (Batman, 2010)

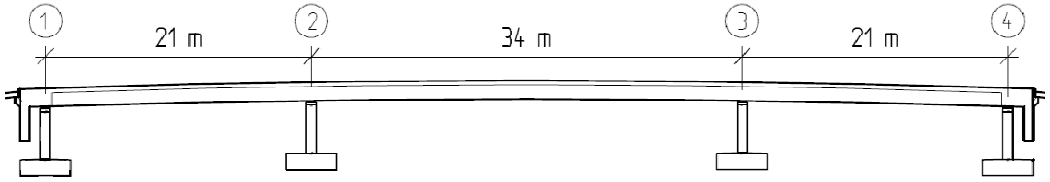

Figure 2.1 Elevation of bridge 16-935-1 at Axevalla over road 49. Adapted from Batman (2010).

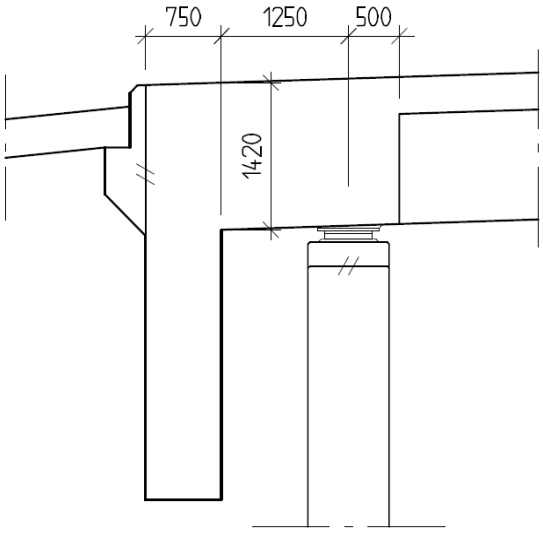

Figure 2.2 Detail of the transversal support beam of bridge 16-935-1 at Axvalla over road 49. Adapted from Batman (2010).

Horizontal displacements in the bearings are restrained in the transversal direction in all supports and support 2 and 3 are also fixed in the longitudinal direction, see Figure 2.3.

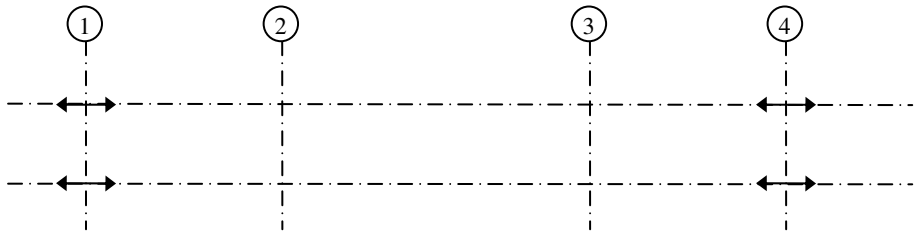

Figure 2.3 Support conditions for bridge 16-935-1, showing the horizontal displacements allowed by the bearings.

The bridge was post-tensioned with an initial prestressing force of 2367 kN per tendon and there are 24 tendons in the bridge, each with a cross sectional area of 1800 mm^2.

After the post-tensioning of the bridge, cracks in the transversal beam were detected. The cracks were located over the bearings at support 1 and 4, see Figure 2.1. The cracks started over the bearings and propagates up and in towards the main beam. A mapping of the cracks was made three weeks after they were first detected, and the mapping was updated three months later. The updated mapping for support 1 is presented in Figure 2.4. At the first mapping, crack 1-2 and 1-4 were not detected, which indicates that these cracks were formed at some time after post-tensioning (Johansson, 2009).

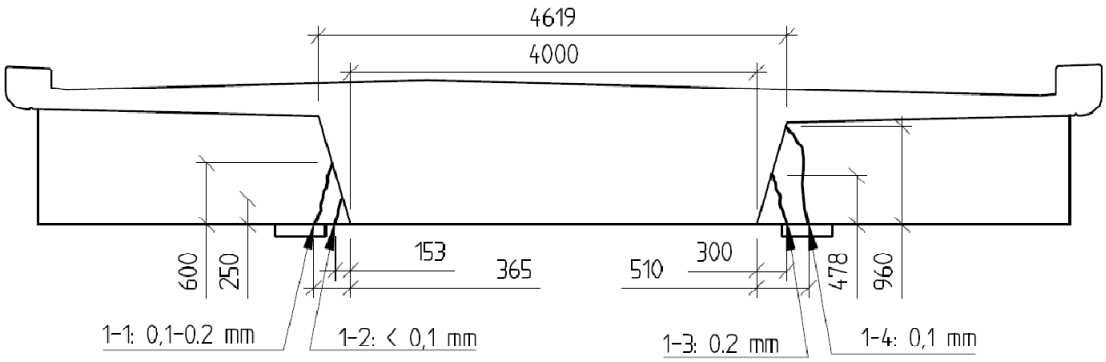

Figure 2.4 Crack mapping of bridge 16-935-1, support 1. Adapted from Batman (2010).

The updated mapping for support 4 is presented in Figure 2.5. Here crack 4-2 and 4-3 was not detected at the first mapping so they have also probably started some time after the post-tensioning of the bridge.

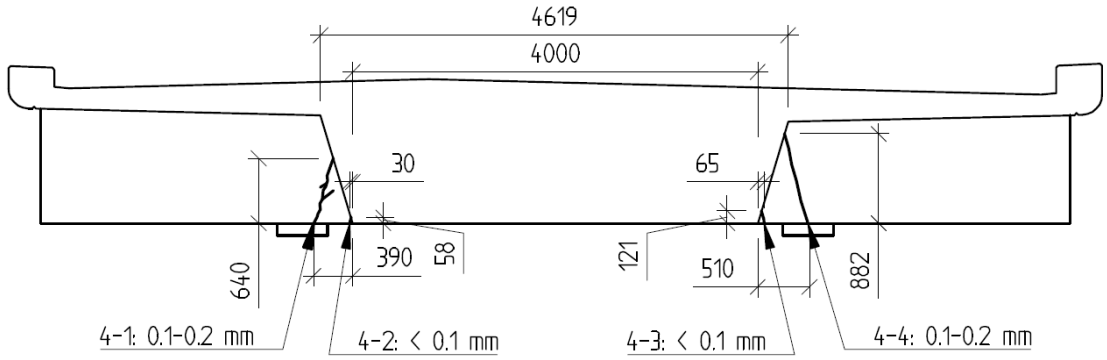

Figure 2.5 Crack mapping of bridge 16-935-1, support 4. Adapted from Batman (2010).

A third mapping was made three months after the second mapping, showing that the cracks look like they did on the second mapping (Johansson, 2009). According to Svensson (2009) the cause of the cracks is the sharp change between the transversal beam and the main beam in combination with long cantilevering parts of the bridge deck slab and the influence of the forces from the post-tensioning. This should give cause to stress concentrations at the surface, in the area where cracks have appeared. Svensson (2009) proposes that, in similar projects the main beam should be gradually broaden towards the transversal beam. He also proposes that the cracks should be injected with epoxy. At the final survey Vägverket stated that the cracks should be mapped every year to monitor if they are propagating or widening.

2.2 Bridge at junction Nol over road 45, 15-1544-1 and -2

Bridge 15-1544-1 and -2, was built during 2009 by the contractor NCC. The bridge is divided into two parts, 15-1544-1 which was designed by Reinertsen and 15-1544-2 which was designed by Vectura. Plans of the structures are presented in Figure 2.6 and Figure 2.7.

Both parts are post-tensioned concrete bridges. Part 15-1544-2 was post-tensioned by 25 tendons with an initial prestressing force of 2367 kN per tendon, each tendon with a cross sectional area of 1800 mm^2. Part 15-1544-1 was post-tensioned by 32 tendons with an initial prestressing force of 2340 kN per tendon, each tendon with a cross sectional area of 1800 mm^2.

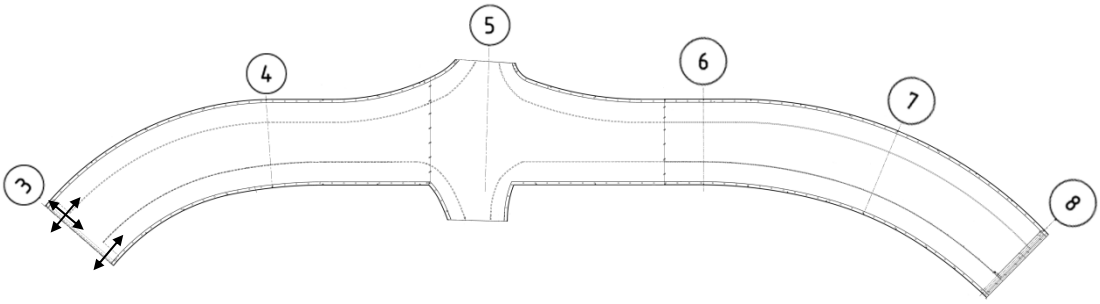

Figure 2.6 Plan of bridge 15-1544-1, showing the horizontal displacements allowed by the bearings at support 3. 15-1544-1 connects to 15-1544-2 at support 3. Adapted from Batman (2010).

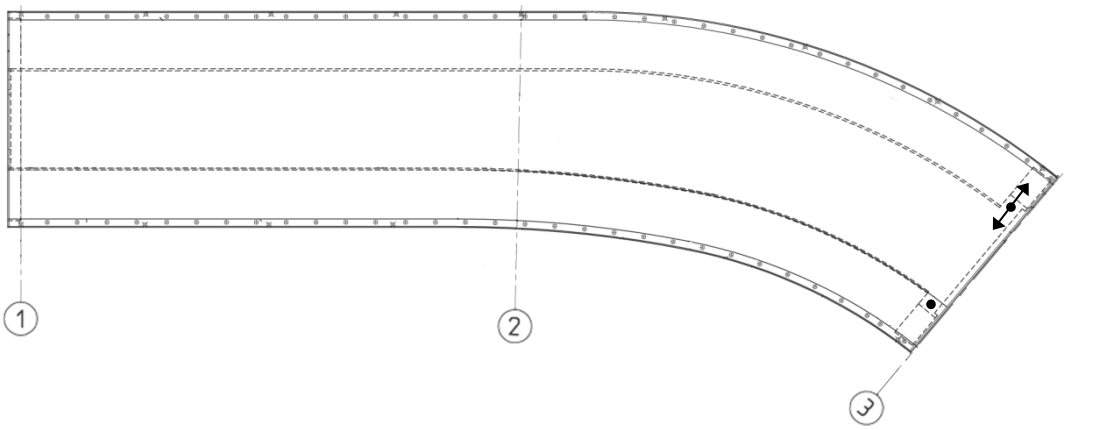

Figure 2.7 Plan of bridge 15-1544-2, showing the horizontal displacements allowed by the bearings at support 3. 15-1544-2 connects to 15-1544-1 at support 3. Adapted from Batman (2010).

The cracks were detected at the transversal beams over support 3 after post-tensioning before the bridge was loaded by traffic. Cracks were only detected on the outside of the curve. The result of the mapping made is presented in Figure 2.8 and Figure 2.9.

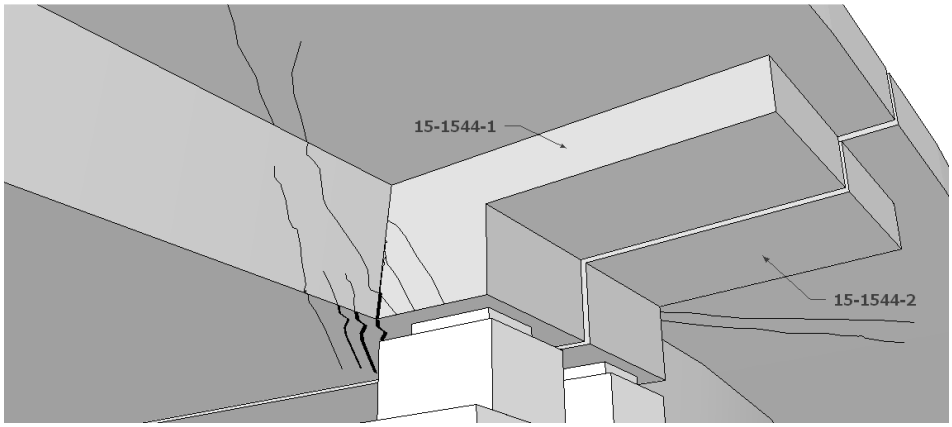

Figure 2.8 Crack mapping of bridge 15-1544-1, support 3. Crack widths: Thick lines, 0.5-0.7 mm, medium lines, 0.3-0.4 mm, thin lines, 0.1-0.2 mm. Adapted from Batman (2010).

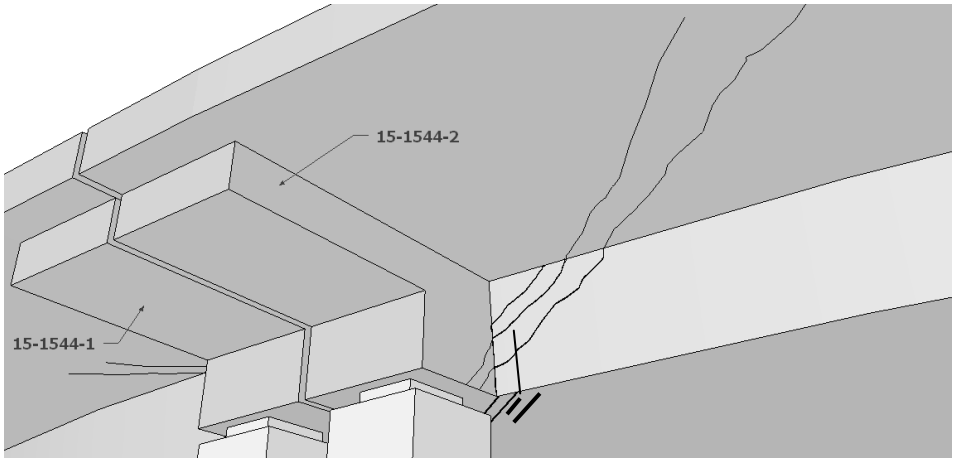

Figure 2.9 Crack mapping of bridge 15-1544-2, support 3. Crack widths: Thick lines, 0.5-0.7 mm, medium lines, 0.3-0.4 mm, thin lines, 0.1-0.2 mm. Adapted from Batman (2010).

2.3 Bridge in Brämhult over road 40, 15-1415-1

Bridge 15-1415-1, located in Brämhult over road 40, was built during 2006 by the contractor PEAB. It is a post-tensioned concrete bridge that consists of two spans with the total length of 26.5 m + 22.5 m = 49 m. The bridge has transversal support beams at each end, see Figure 2.10 for elevation of the bridge and Figure 2.11 for detail of the transversal beam. The bridge was designed by Inhouse Tech.

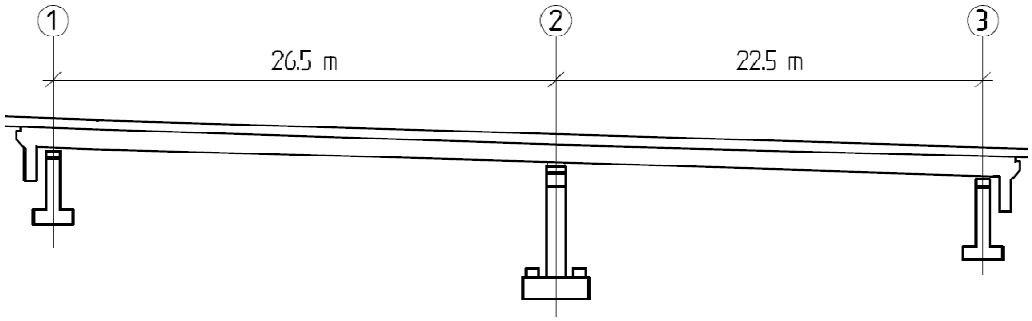

Figure 2.10 Elevation of bridge P1514 at Brämhult over road 40. Adapted from Batman (2010).

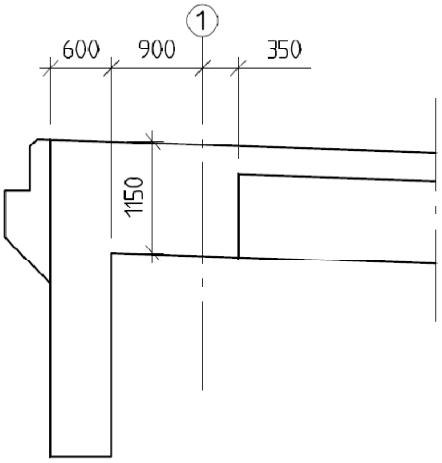

Figure 2.11 Detail of the transversal support beam of bridge P1514 at Brämhult over road 40. Adapted from Batman (2010).

Support conditions concerning directions of possible horizontal displacements are presented in Figure 2.12. The arrangement of the bearings is made so that no restraint is obtained between the bearings. The bridge is post-tensioned by 18 tendons, each with a cross section area of 1800 mm^2 and the initial prestressing force per tendon is 2376 kN per tendon (Batman, 2009).

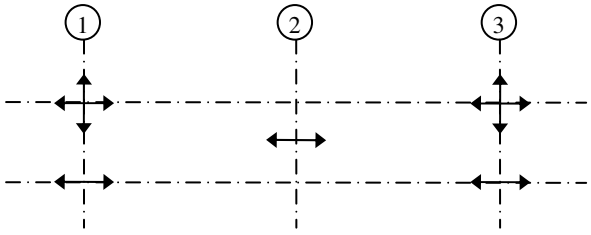

Figure 2.12 Support conditions for bridge 15-1415-1, showing the horizontal displacements allowed by the bearings.

Cracks were detected in the transversal beams at support 1 and 3 before it was loaded with traffic. A mapping of the cracks was made and the results are presented in Figure 2.13 for support 1 and Figure 2.14 for support 3. The crack widths were measured to be between 0.05 mm and 0.1 mm. (Migell, 2006)

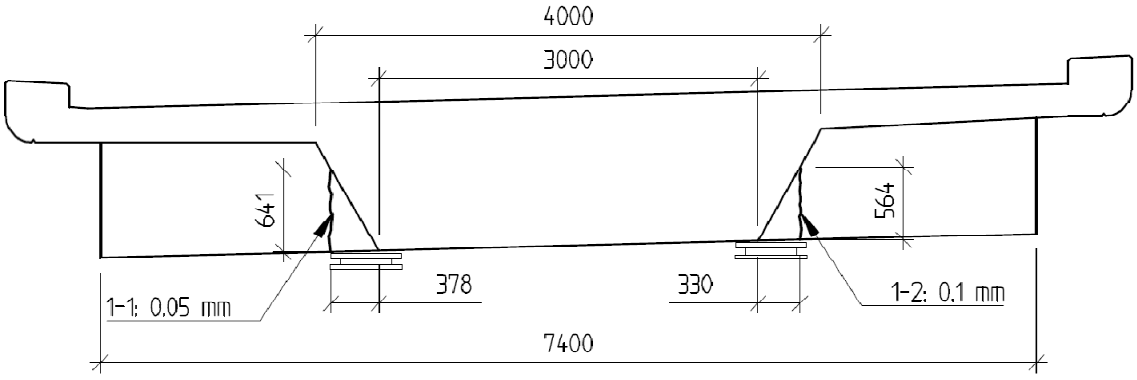

Figure 2.13 Crack mapping of bridge P1514, support 1.

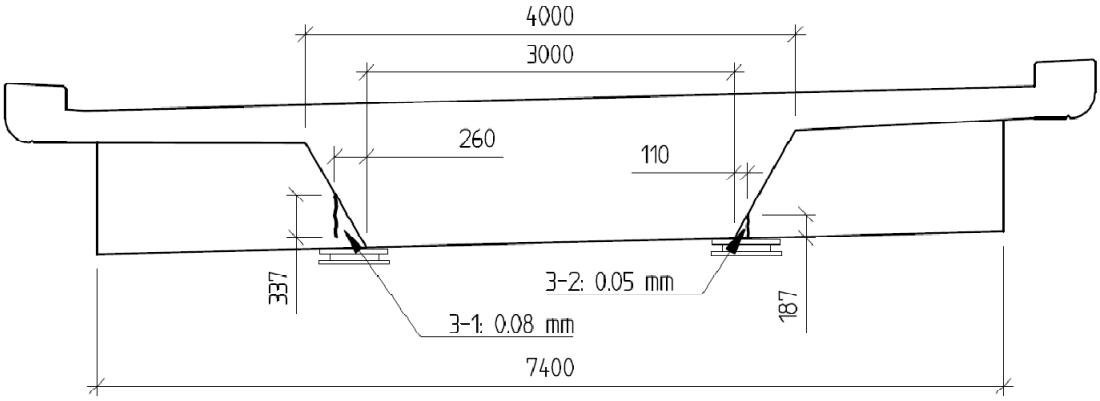

Figure 2.14 Crack mapping of bridge P1514, support 3.

Further inspections were made and it was stated that the cracks had not increased in numbers, width or length. The designer could not see that the design of the bridge should have caused the bridge to crack. They state that temperature probably not caused the cracks since no restraint exists for the transversal beam. The designer also states that stresses will appear at the front face of the transversal beam at post-tensioning, but these stresses are not assumed to be large enough to cause cracks. Moments, shear forces or spalling forces should neither be enough to cause cracks in the region. (Migell, 2006)

2.4 Bridge in Gulbranna over road E6, 13-799-1

The bridge, situated in Gulbranna in Halmstad län, was built by the contractor SIAB in 1994. The company that designed the bridge was Centerlöf and Holmberg. It is a post-tensioned concrete bridge that consists of two spans with the total length L = 29 m + 29 m = 58 m. It has transversal support beams over each end support; see Figure 2.15 for elevation of the bridge and Figure 2.16 for detail of the transversal beam. (Batman, 2010)

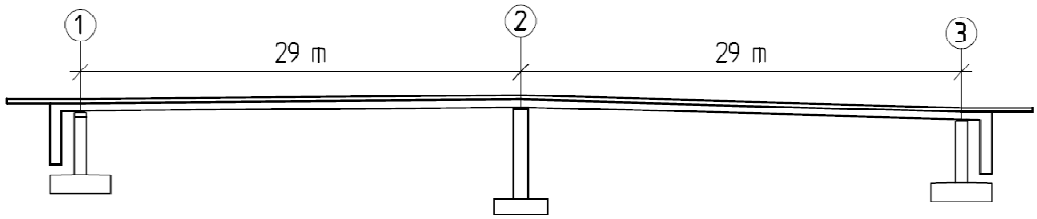

Figure 2.15 Elevation of bridge 13-799-1 in Gulbranna. Adapted from Batman (2010).

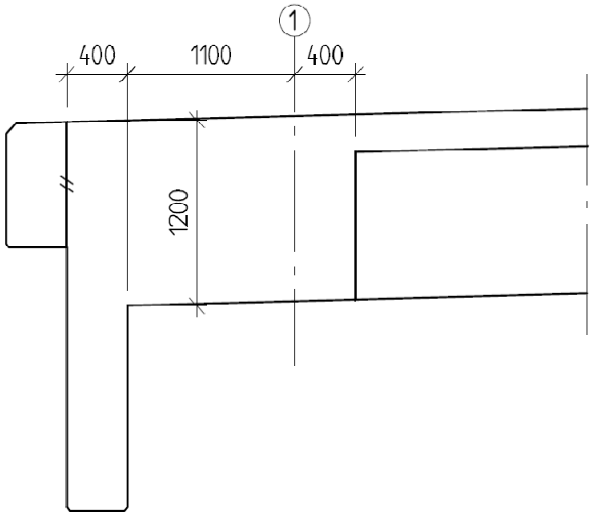

Figure 2.16 Detail of the transversal support beam of bridge 13-799-1 in Gulbranna. Adapted from Batman (2010).

Support 1 and 3 are free to move in the longitudinal direction, but fixed in the transversal direction. Support 2 is fixed in both longitudinal and transversal direction, see Figure 2.17.

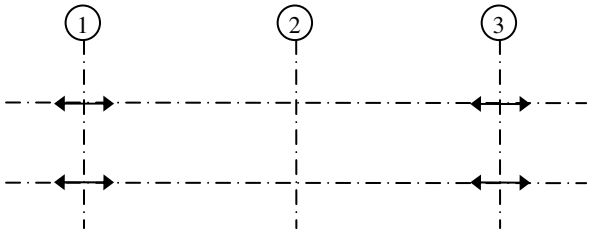

Figure 2.17 Support conditions for bridge 13-799-1.

Cracking occurred at the transversal beam at support 1 and 3. The bridge was loaded by traffic in April 1994, and the cracks were mapped only a few days later. However, it is most likely that the cracks have developed before the bridge was loaded by traffic because of the fact that the other bridges described in this report has all cracked before they were loaded with traffic. The crack widths were measured to between 0.1-0.3 mm and the mapping can be seen for support 1 in Figure 2.18 and for support 3 in Figure 2.19. No information exists of what the designer thinks have caused the cracks. (Jarlsson, 1994)

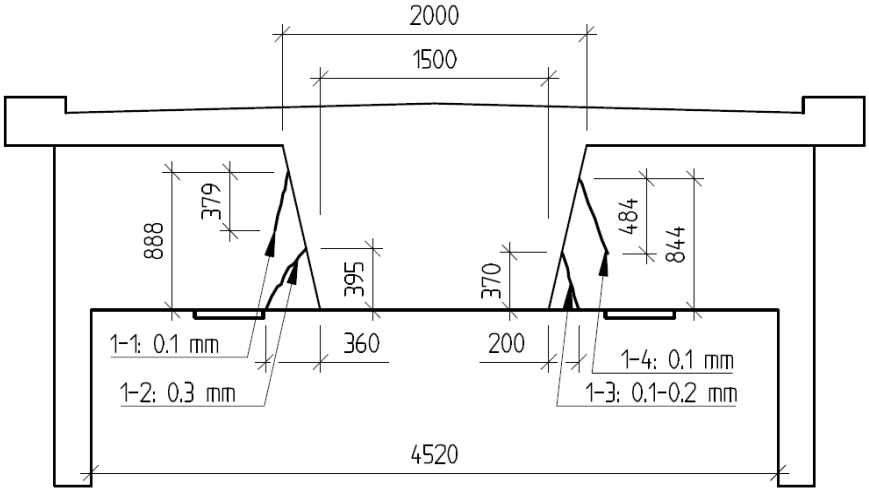

Figure 2.18 Crack mapping of bridge 13-799-1, support 1. Adapted from Batman (2010).

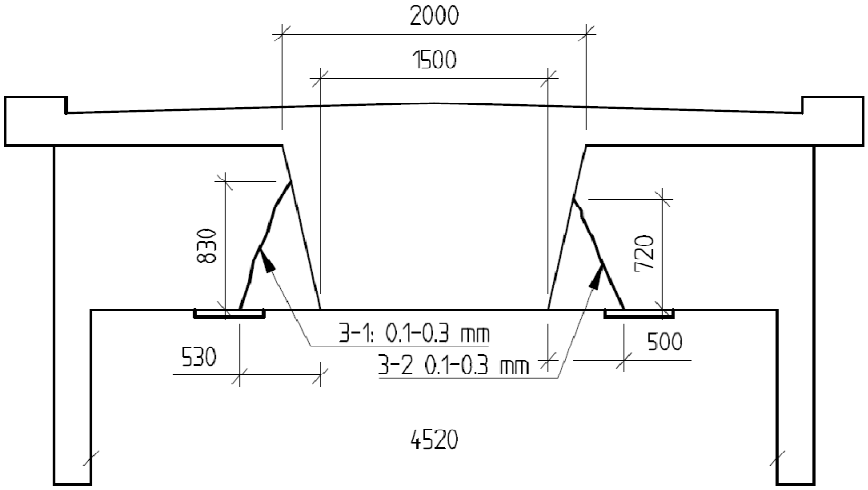

Figure 2.19 Crack mapping of bridge 13-799-1, support 3. Adapted from Batman (2010).

3 Transversal support beams

Since all the bridges studied in chapter 2 have experienced cracking in their transversal support beams, a short description of the commonly used design procedure for the transversal beams is presented in section 3.1. The purpose of this section is to show which loads that are included, and what the simplified model used in the design looks like. A comparison with the design procedure used in Eurocode is not included since the same load cases and the same structural model can be used irrespectively of if the Swedish code or Eurocode is used. The choice of structural model is up to the designer, and is not regulated in the codes.

Since all the bridges studied in this report most likely have cracked before they were loaded by traffic loads, hand calculations are performed to see if it is likely that the beams have cracked by the self-weight. A description of how the hand calculations were performed and the result of these are presented in section 3.2.

3.1 Design procedure for transversal support beams

Based on the bridges studied in chapter 2, the design procedure for transversal support beams of the type studied in this thesis are in general the same, independently of which company that have designed the bridge. The general procedure is as follows:

1. Make a global analysis of the bridge to find the load case in ultimate limit state which gives the largest reaction force, R, in the considered support.
2. Assume a 2D-model of the transversal beam according to Figure 3.1. The distributed load q acting on the transversal beam is obtained by assuming that the load acting on the bridge is distributed over the width of the main beam, l_{mb}. The distributed load is then calculated as $q = R / l_{mb}$. In cases where torsional moments are present in the main beam over the support, these must be accounted for when determining the load acting on the transversal beam.
3. The transversal beam is then designed in the ultimate limit state, either as an ordinary beam or as a deep beam according to BBK 04 (Boverket, 2004) section 6.6.
4. According to Vägverket (2007), section 42.322, the steel yield strength f_{st} should be limited to 250 MPa in the ultimate limit state design of deep beams, in order to limit the crack widths. If this reduction of the design steel strength is made, no further checks of crack widths in the deep beam for service state is needed. This applies to both transversal and vertical reinforcement. For ordinary beams crack widths should be checked according to BBK 04 (Boverket, 2004).

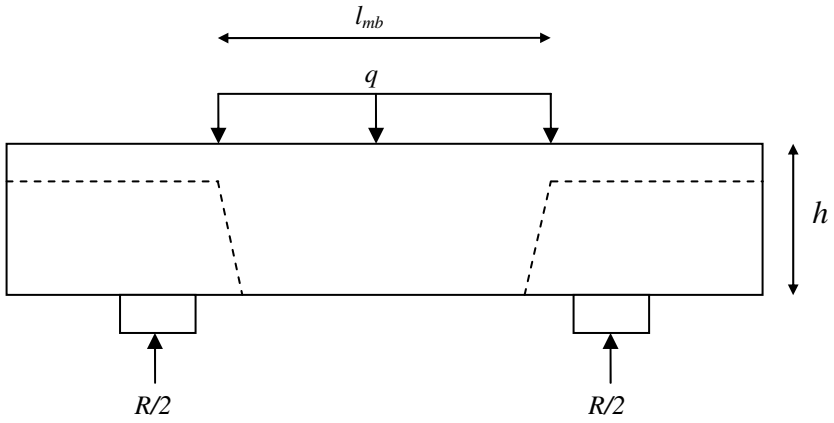

Figure 3.1 Load and boundary conditions commonly used in the design of transversal support beams.

As stated above, the design procedure of the transversal beam is different if the beam is regarded as a deep beam or not. The ratio that should be fulfilled to regard the beam as a deep beam is:

$$\frac{M_0}{hV_0} \leq 1.5 \tag{3.1}$$

where

M_0 is the bending moment in field assuming the beam as simply supported on the two supports.

V_0 is the shear force at support assuming the beam as simply supported on the two supports.

h is the total height of the transversal beam.

The design in ultimate limit state used for deep beams as well as ordinary beams can be studied in the Swedish code BBK 04 (Boverket, 2004) together with some additional rules given by the Swedish road administration (Vägverket, 2007).

3.2 Hand calculations of bridge 16-935-1

In order to see if it is likely that the bridges have cracked just by the self-weight, hand calculations is performed on the bridge at junction Axevalla, 16-935-1. This is the same bridge that is later used as case study in the FE-analysis, see chapter 5. The following hand calculations are made to see if the maximum principal stresses exceeds the characteristic tensile strength of concrete, 5th percentile value. Since the transversal beam is considered not to be a deep beam according to equation (3.1), Euler-Bernoulli beam theory is assumed.

The calculations were performed in MathCAD and were executed in the following way.

1. A global analysis is performed to obtain the total reaction force at the supports below the transversal beam.
2. The load at the transversal beam is assumed to act in the same way as described in point 2 in chapter 3.1.
3. The moment and shear force distribution along the transversal beam is calculated using the 2D-model presented in Figure 3.1.

4. The stresses along the transversal beam is calculated according to theory of elasticity:

$$\sigma(x,z) = \frac{M(x)}{I_{tb}} \cdot (z_{GC} - z) \tag{3.2}$$

$$\tau(x,z) = \frac{S(z) \cdot V(x)}{I_{tb} \cdot t_{tb}} \tag{3.3}$$

Where

$\sigma(x,z)$ is the normal stress due to bending moment.

$\tau(x,z)$ is the shear stress.

$M(x)$ is the moment along the transversal beam.

I_{tb} is the second moment of area of the transversal beam.

$S(z)$ is the first moment of area.

x is the length coordinate of the transversal beam, starting at the left bearing.

z is the distance from the bottom of the transversal beam.

z_{GC} is the position of the gravity centre of the cross-section, measured from the bottom of the beam.

t_{tb} is the thickness of the transversal beam.

5. Using equation (3.2) and (3.3) the maximum principal stresses at various height of the transversal beam is calculated according to the following expression:

$$\sigma_1(x,z) = \frac{\sigma(x,z) + \sigma_z}{2} + \sqrt{\left(\frac{1}{2} \cdot (\sigma(x,z) - \sigma_z)\right)^2 + \tau(x,z)^2} \tag{3.4}$$

Where

$\sigma_1(x,z)$ is the maximum principal stress.

σ_z is the normal stress in vertical direction, which is zero according to beam theory.

Using the procedure above with the static model presented in Figure 3.2 the maximum principal stresses at different heights of the transversal beam is calculated for the chosen bridge; see Appendix A1 and Appendix A2. The result together with the tensile strength of concrete, 5th percentile value, is presented in Figure 3.3.

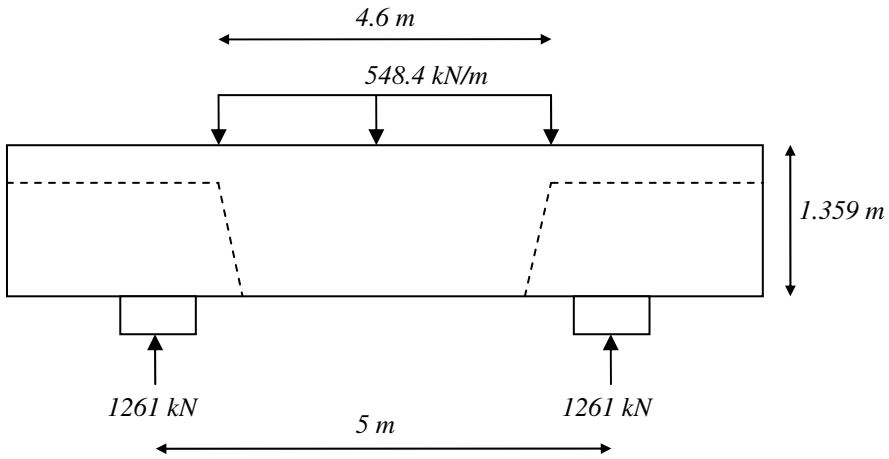

Figure 3.2 Structural model used in hand calculation of principal stresses for the transversal beam of bridge 16-935-1.

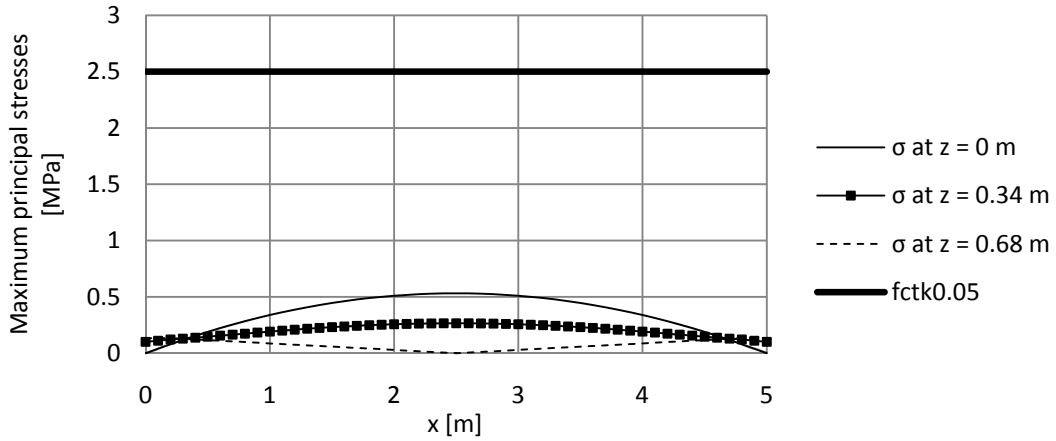

Figure 3.3 Maximum principal stresses along the transversal beam.

These results show that it is a very small possibility that the transversal beam have cracked from the self-weight when a 2D-model is used for calculation. The tensile strength of the concrete is much larger than the maximum principal stresses according to beam theory. This shows that a large increase of the load or a large decrease of the tensile strength must occur in order to get cracking of the transversal beams due to vertical loading.

4 FE – modelling theory

4.1 Concrete material models

Since the FE-analysis should be able to describe the behaviour of reinforced concrete in the cracked state a non-linear material model must be used. In BRIGADE/Plus there are two different material models that can be used to simulate the non-linear behaviour of concrete, the damaged plasticity model and the smeared cracking model. The first model is based on the theory of plasticity and the most stable one. The latter method is based on the theory of fracture mechanics. (Simulia, 2009a) The damaged plasticity model is the one used in the FE-analyses described in this report and the model is described in chapter 4.1.3.

To give a better understanding of how the concrete model are constructed the tensile behaviour of concrete is treated in section 4.1.1, and the compressive behaviour is treated in section 4.1.2.

4.1.1 Tensile behaviour of concrete

When a concrete specimen is subjected to a deformation controlled tensile test, it will elongate elastically until the tensile strength, f_{ct}, is reached. A macro crack will then localize from several micro cracks concentrated to the weakest zone of the specimen. The elongation of the specimen is now determined from both the elastic elongation in uncracked regions and the crack opening in the cracked region of the specimen. As the crack propagates, the uncracked regions are unloaded, and the elastic elongation in these regions eventually goes to zero. The final elongation of the specimen is therefore only determined by the width of the crack, w. If the test is to be described in terms of a stress-strain relation, it will result in a size dependency which makes the test unable to describe a general situation. To handle this problem, the test must instead be described in terms of a stress-strain relation for uncracked regions, and a stress-crack opening relation for the cracked zone. The primary material parameter which is used to characterize the tensile behaviour of concrete after cracking is the fracture energy, G_f. The fracture energy is the area under the stress-crack opening curve, and it corresponds to the energy consumed during the fracture process from zero crack opening to splitting of the specimen. Figure 4.1 shows the schematic relation between tensile stress, crack opening and fracture energy. (Plos, 2000)

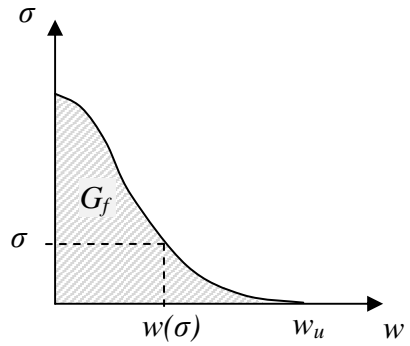

Figure 4.1 Schematic stress-crack opening relation for concrete. Adapted from Plos (2000).

Several studies have been made to quantify the tensile behaviour of concrete in terms of the curve and parameters presented in Figure 4.1. The following text present some of these.

Recommendations given by CEB (1993) for how the fracture energy should be chosen, depending on the strength class and maximum aggregate size of the concrete, are presented in Table 4.1.

Table 4.1 Fracture energy for concrete classes C12-C80. (CEB, 1993)

Max aggregate size [mm]	G_f [Nm/m^2]							
	C12	C20	C30	C40	C50	C60	C70	C80
8	40	50	65	70	85	95	105	115
16	50	60	75	90	105	115	125	135
32	60	80	95	115	130	145	160	175

The shape of the stress-crack opening curve can be approximated numerically with different accuracy. The simplest approximation is the linear decrease of stress with increasing crack opening as shown in Figure 4.2a. The ultimate crack opening w_u can then be calculated from the fracture energy and the concrete tensile strength f_{ct} according to the following equation.

$$w_u = \frac{2G_f}{f_{ct}} \tag{4.1}$$

A more accurate representation of the real behaviour is obtained if a bi-linear stress-crack opening curve is used. Such an approximation is proposed by Hillerborg (1986), where the breakpoint in the bi-linear curve is determined according to Figure 4.2b. The most accurate approximation of the real behaviour is probably an exponential decrease of stress with increasing crack opening, see Figure 4.2c. Such a model has been developed by Cornelissen et al. (1986). The mathematical model relates the stress, σ, to the crack opening, w, according to the following equations:

$$\frac{\sigma}{f_{ct}} = f(w) - \frac{w}{w_u} f(w = w_u) \tag{4.2}$$

$$f(w) = \left[1 + \left(C_1 \frac{w}{w_u}\right)^3\right] \cdot e^{-C_2 \frac{w}{w_u}} \tag{4.3}$$

Where

w_u is the crack opening for which stress no longer can be transferred.
w_u = 160 μm for normal weight concrete.

C_1 is a material constant.
C_1 = 3 for normal weight concrete.

C_2 is a material constant.
C_2 = 6.93 for normal weight concrete.

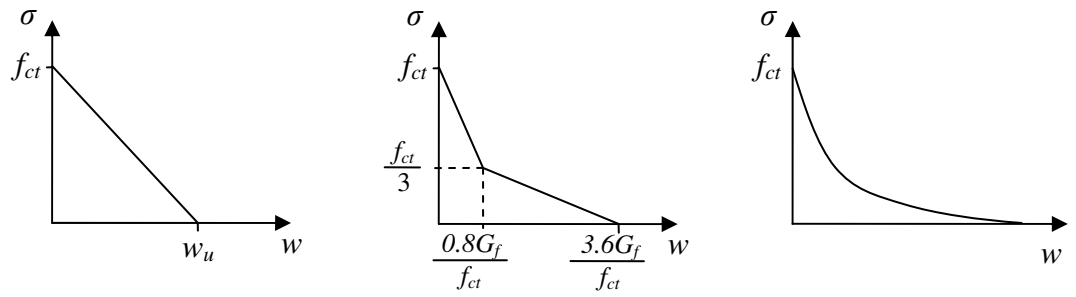

Figure 4.2 Linear, bi-linear (Hillerborg, 1986) and exponential (Cornelissen et al., 1986) representation of the stress-crack opening relationship for concrete.

4.1.2 Compressive behaviour of concrete

The compressive behaviour of concrete is in general calculations idealized to be linear elastic. A more realistic representation of the stress-strain behaviour, which should be used in non-linear structural analysis, is given in EN 1992-1-1 (2004), see Figure 4.3, were also the linear behaviour is represented by the straight line. The stress-strain curve is obtained from the following equations:

$$\frac{\sigma_{cc}}{f_{cm}} = \frac{k\eta - \eta^2}{1 + (k-2)\eta} \tag{4.4}$$

$$\eta = \frac{\varepsilon_{cc}}{\varepsilon_{cc1}} \tag{4.5}$$

$$k = 1.05 E_{cm} \frac{\varepsilon_{c1}}{f_{cm}} \tag{4.6}$$

where

σ_{cc} is the concrete compressive stress.

ε_{cc} is the concrete compressive strain.

f_{cm} is the mean value of the concrete compressive strength.

ε_{cc1} is the concrete compressive strain when $\sigma_{cc} = f_{cm}$.

E_{cm} is the mean value of the Young's modulus of concrete.

This relation is valid for uniaxial, short-term loading in the strain range $0 < \varepsilon_c < \varepsilon_{cu1}$, where ε_{cu1} is the nominal ultimate strain.

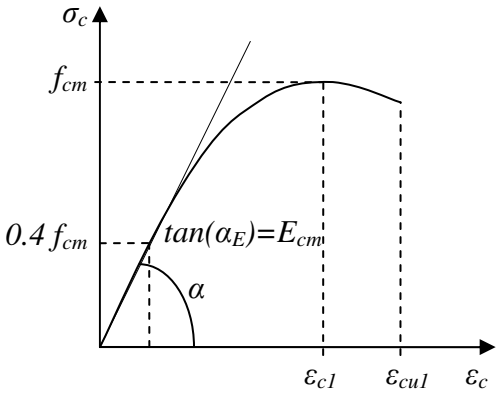

Figure 4.3 Stress-strain relation for concrete in compression. Adapted from EN 1992-1-1 (2004).

4.1.3 Concrete damaged plasticity

The concrete damaged plasticity model is the more stable of the two concrete models that are included in BRIGADE/Plus and it is the most commonly used according to Kölfors[1]. It is used for modelling concrete that is subjected either to cyclic, dynamic or monotonic loading under low confining pressure. The model is based on the theory of plasticity and assumes that the two failure mechanisms are cracking or crushing of the concrete. Initially the material has a linear stress-strain relation but when the yield surface, which defines when the deformations become plastic, is reached the strain is subdivided in an elastic part, ε_{el}, and a plastic part, ε_{pl}. The yield surface for plane stress states used in the concrete damaged plasticity model can be seen in Figure 4.4. (Simulia, 2009a)

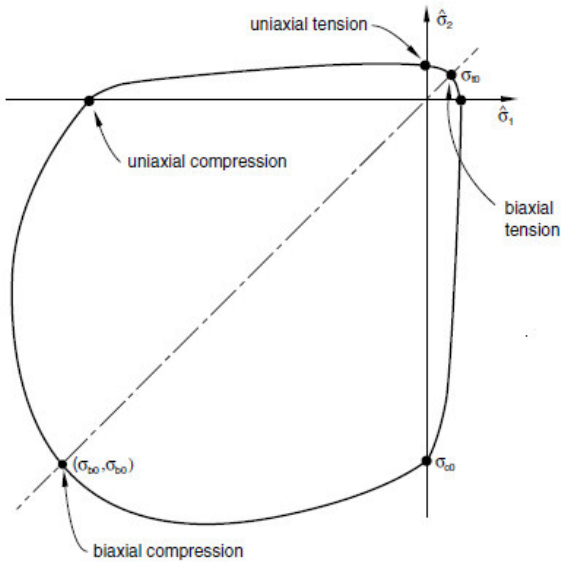

Figure 4.4 Yield surface for plane stress (Simulia, 2009a).

When the initial yield stress in compression, σ_{c0}, is reached the materials stiffness decreases until the ultimate stress, σ_{cu}, is reached. After that the strain increases with

[1] Johan Kölfors, Scanscot Technology, 2010-02-17

decreasing stress. The concrete response for uniaxial compression is presented in Figure 4.5 where d_c is a variable between 0 and 1 which defines how large the stiffness decrease is. (Simulia, 2009b)

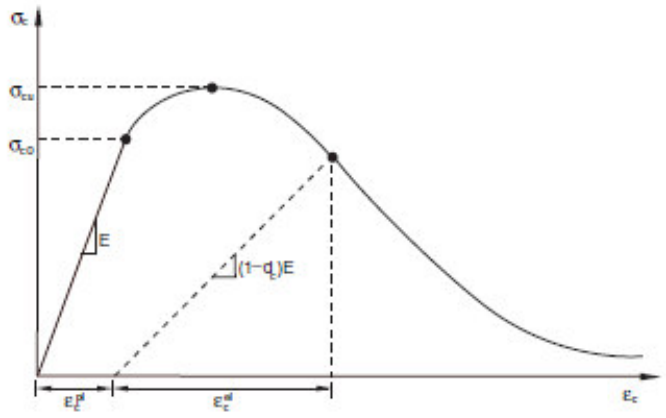

Figure 4.5 Uniaxial compressive behaviour (Simulia, 2009b).

When the initial yield stress in tension, σ_{t0}, is reached the material loses stiffness and the total strain increases with decreasing stress. The concrete response for uniaxial tension is presented in Figure 4.6 where d_t is a variable between 0 and 1 which defines how large the stiffness decrease is. (Simulia, 2009b)

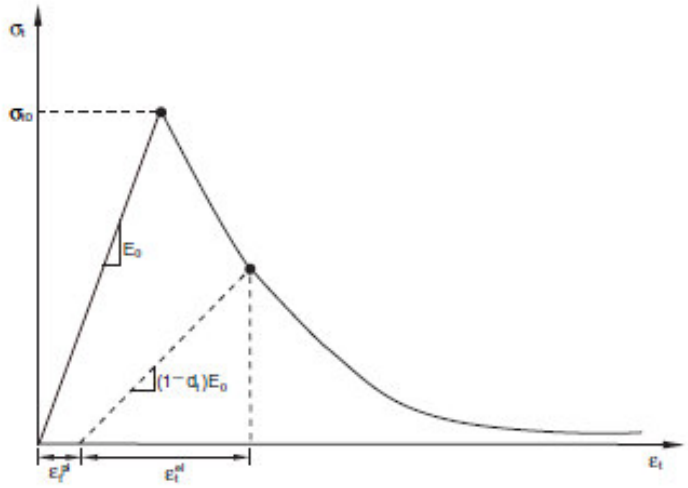

Figure 4.6 Uniaxial tensile behaviour (Simulia, 2009b).

When using the damaged plasticity model the post failure compressive and tensile behaviours need to be defined. The post failure behaviour in compression is defined as a stress – plastic strain relation. In tension the post failure behaviour is defined by the tension softening behaviour. This behaviour can be defined according to any of the curves in Figure 4.2, with a stress-displacement relation. The advantage of defining the tension softening behaviour with a stress-displacement relation instead of a stress-strain relation is that the tensile response becomes less mesh dependent. If a stress-displacement relation is defined, the crack band width is chosen by BRIGADE/Plus to the characteristic crack length. The characteristic crack length is typically half of the length across one element for second order solid elements.

The compressive strength of concrete is increasing with increasing hydrostatic compressive pressure. When using the material model described in this chapter two

parameters that describe the relation between hydrostatic pressure and the strength of concrete needs to be defined. These are the dilation angle, ψ, which should be in the interval of 32° and 38° according to Kölfors[2], and the eccentricity, ε, which is a small positive value with the default value 0.1 in BRIGADE/Plus. (Simulia, 2009a)

The compressive and tensile behaviour is defined for uniaxial stress state. For the program to translate these values into a biaxial stress state relation the ratio between the initial equibiaxial compressive yield stress and the initial uniaxial compressive yield stress, σ_{b0}/σ_{c0} needs to be defined. The default value of this ratio is 1,16. To be able to describe the yield surface in the deviatoric plane K_c is defined. For different values of K_c the yield surface in the deviatoric plane changes, see Figure 4.7. K_c should be in the range of $0{,}5 < K_c < 1.0$ and the default value is 2/3. (Simulia, 2009a)

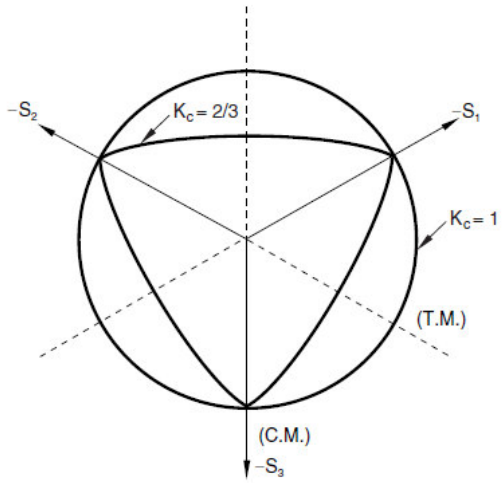

Figure 4.7 Typical yield surface in the deviatoric plane for different values of K_c, (Simulia, 2009b)

When the response of the model corresponds to a decrease of the stiffness, convergence problems often occurs. This can be avoided using a viscoplastic adjustment, μ, of the constitutive relation. Then the stresses are allowed to be outside the yield surface and convergence problems might be avoided. If such an adjustment should be used, μ should be defined as a small positive value. If no viscoplastic adjustment should be included μ is defined as zero which is the default value. (Simulia, 2009b)

4.2 Element types

A number of different element types exist in most finite element codes. These have different properties and are good in describing various behaviours. For structural analysis the most commonly used element types are solid, beam, shell and truss elements. Shell elements are used to model a structure when one thickness of the member is much smaller than the others, for example a plate. Shell elements are not used in the FE-model described in this thesis and are not treated further in this report. The following sections will give a short introduction to solid, beam and truss elements.

[2] Johan Kölfors, Scanscot Technology, 2010-02-17

4.2.1 Solid elements

Solid elements can be used when the model is either in 2D or 3D. In the general 3D cases each node has three degrees of freedom, DOFs, which are translations in x-, y-, and z-direction, see Figure 4.8. Elements with nodes only in the corners are called first order elements and uses linear interpolation to obtain a solution. Elements with nodes at corners and additional nodes at the mid-point of each edge use quadratic interpolation and are called second order elements.

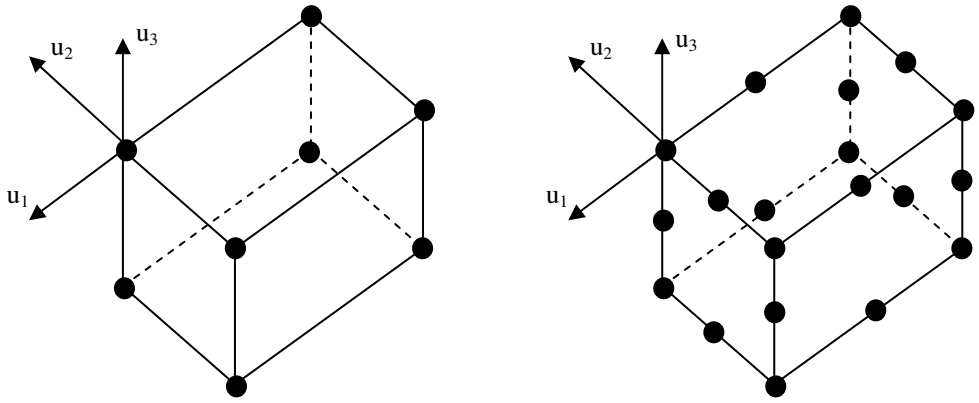

Figure 4.8 First order hexahedral solid element and second order hexahedral solid element.

Second order elements are more expensive in terms of computational cost, but are better to describe bending. Solid elements are good to describe shear failure and good to use when an arbitrary geometry exists. Its disadvantage is that the computational cost is larger than for beams and shell elements.

In the FE-models described in this report two different solid elements were used. They are in BRIGADE/Plus defined as C3D20 and C3D20R. Both element types are 3D solid elements with 20 nodes, which mean that they use quadratic interpolation. The difference between the elements is that C3D20R uses reduced integration. C3D20 uses 27 integration points and C3D20R uses 8 integration points, this means that the computational cost is lower for C3D20R. Where stress or strain concentrations may exist, e.g. in concrete that cracks, a fully integrated element, C3D20, provides the best solution. (Simulia, 2009a)

4.2.2 Beam elements

A beam element can be used in both 2D and 3D models. A 3D beam element has 6 DOFs at each node: rotations and translations in x-, y-, and z-directions. A first order beam element consists of one node at each end and a second order beam element also contains a node at the middle of the element, see

Figure 4.9. The beam elements are based on Euler-Bernoulli or Timoshenko beam theory. They are good to describe bending but they cannot describe failure due to shear. An advantage is that it takes low computational cost to use beam elements.

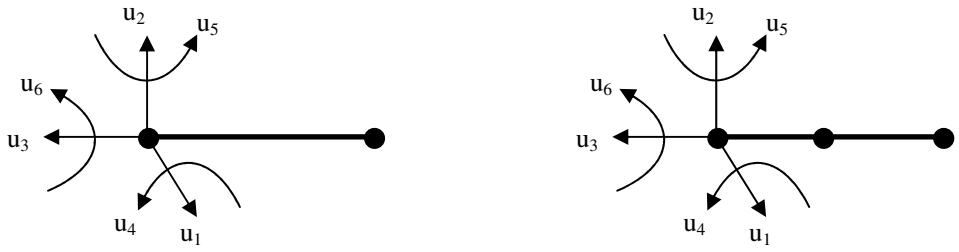

Figure 4.9 First order beam element to the left, second order beam element to the right.

In the FE-model described in this report one type of beam element is used. It is in BRIGADE/Plus defined as B31. It is a first order 3D beam element which is based on Euler-Bernoulli beam theory. These elements should be used when the cross-sectional area is small compared to the span length which is the case in the model described in this report. (Simulia, 2009a)

4.2.3 Truss elements

Truss elements are 2D or 3D elements that are good to describe long slender geometry, which can be assumed to have no stiffness in its transversal direction. It has only one DOF per node that describes the translation in the axial direction, see Figure 4.10. The truss elements are good to use for the reinforcement in an FE-analysis of reinforced concrete.

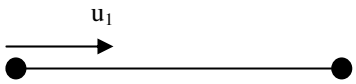

Figure 4.10 Schematic representation of a truss element.

In the model described in this report one type of truss element is used. It is in BRIGADE/Plus defined as T3D2. T3D2 is a 3-dimensional element that consists of two nodes and it use linear interpolation to obtain a solution. (Simulia, 2009a)

4.3 Interaction between parts of the FE-model

In order to reduce the computational cost of an FE-analysis one part of the model can be modelled with beam elements while the part of interest for studying of detailed results is modelled more detailed with solid elements. A tie constraint can then be defined between the different parts to transfer displacements and forces from one part to another. BRIGADE/Plus provides some built in tie constraints. In the analysis made the “surface to surface” constraint is used.

The “surface to surface” constraint defines a slave surface and a master surface which are tied together. The slave surface will obtain the same values for is DOFs as the master surface. If a beam element that has three translational and three rotational DOFs are tied to a solid element with only three rotational DOFs the solid part will obtain the translational DOFs, and the rotational DOFs will be transformed to translational DOFs using the offset distance between the surfaces as the lever arm. “Surface to surface” constraints can also be used between parts with the same element

type but with different meshes, in that case the part with the finest mesh should be defined as the slave surface.

In a constraint between two parts, unreasonable stress concentrations might occur, so care must be taken on where to place the constraint in order to avoid numerical problems in case of a non-linear analysis. (Simulia, 2009a)

4.4 Reinforcement

For reinforcement either elastic or plastic material models can be used. If the model should be loaded until collapse, a plastic material model which includes the yielding and strain hardening of the steel is needed. The analysis treated in this report is only describing the behaviour in the service state and the yielding and strain hardening is not included in the model. For modelling the interaction between steel and surrounding reinforcement BRIGADE/Plus provides the "embedded elements" constraint, it means that full interaction is used between reinforcement and concrete. To include the effect of bond-slip in the model it might be possible to include spring elements between reinforcement and concrete that describes the bond-slip relation. Reinforcement can be modelled with solid, beam or truss elements depending on what the analysis focuses on to describe. The most commonly used element type is however truss elements if the "embedded elements" constraint is used.

In the FE-model described in this report the reinforcement is modelled with truss elements and with the "embedded elements" constraint. When the node of an embedded element, the reinforcement, lies in a host element, the concrete, the DOFs of the reinforcement are tied to the corresponding DOFs of the concrete. (Simulia, 2009a)

4.5 Prestressing

In BRIGADE/Plus there is a built in function for defining the prestressing tendons. By entering the coordinates of the tendons and the cross-sectional area the tendons will obtain their position in the model and they can be placed either in beam, shell or solid elements. The tendons are modelled by truss elements and are tied to beam host elements with the "node to surface" constraint, which works in a similar way as the "surface to surface" constraint described in section 4.2.4. Tendons which lie in solid host elements are tied to their host elements using the "embedded elements" constraint described briefly in section 4.4.

The post-tensioning force and the allowed tendon force after anchoring are defined together with the friction coefficient, μ, and the unintended inclination of the tendons, k. BRIGADE/Plus then use these values to calculate a fictitious temperature distribution along each tendon according to the following expressions for friction loss and translation from stress to temperature.

$$P_i(s) = P_i(0)e^{-(\mu \cdot \alpha + k \cdot s)} \tag{4.7}$$

$$T(s) = \frac{P_i(s)}{\alpha_e \cdot E \cdot A_t} \tag{4.8}$$

Where

$P_i(s)$ is the initial prestressing force at the coordinate s.

$T(s)$ is the fictitious temperature in the tendon at the coordinate s.

s is the length coordinate of the tendon from the active end to the section under consideration.

α is the change of slope over the distance s.

α_e is the thermal expansion coefficient.
$\alpha_e = 1.2 \cdot 10^{-5}$ in BRIGADE/Plus.

E is the Young´s modulus of the tensioning steel.

A_t is the cross-sectional area of one tendon.

The fictitious temperature field calculated is applied to the tendons as the analysis proceeds, causing stresses corresponding to the prestressing force.

4.6 Non-linear FE-analysis

In order to obtain a solution in a FE-analysis which exhibits a non-linear response an incremental iterative solution method must be used. BRIGADE/Plus uses Newton's method as the standard method to solve the non-linear equilibrium equations. This is briefly described below. Alternative methods for solving non-linear problems are the modified Newton method and several quasi-Newton methods, which were not be used in this study and are not further treated.

Incrementation in BRIGADE/Plus is made with load control or displacement control for static stress analyses of the type used in this study. Load control means that the solver searches the solution for a certain load in each increment, finding the corresponding displacements which yields equilibrium to the system. The opposite situation is called displacement control, see Figure 4.11.

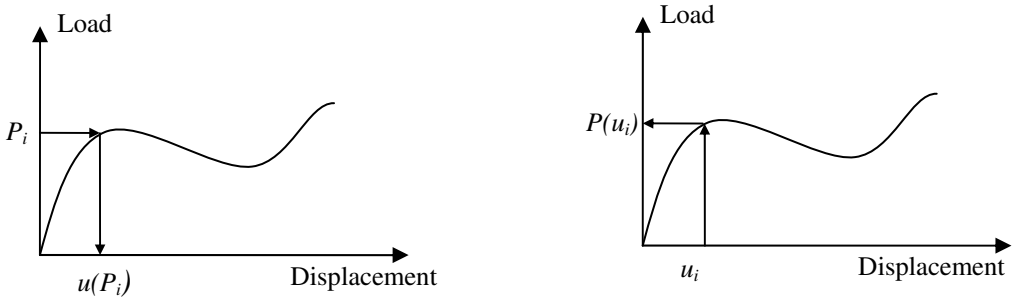

Figure 4.11 Load controlled incrementation to the left and displacement controlled incrementation to the right.

In each increment, the iterative solution method searches for equilibrium. Newton's method uses the following scheme, which is schematically described in Figure 4.12.

1. Each increment starts by calculating the tangent stiffness K_0, based on the current configuration of the system (where P_a and u_0 are obtained from the previous increment).
2. By using the tangent stiffness, the displacement correction, c_i, corresponding to the load increase ΔP is calculated.
3. The new configuration of the system, u_{i+1}, is obtained by adding the displacement correction to the current configuration.

$$u_{i+1} = u_i + c_{i+1} \tag{4.9}$$

4. The internal force of the system, I_{i+1}, is calculated and the force residual, R_{i+1}, for the iteration is obtained as

$$R_{i+1} = P_b - I_{i+1} \tag{4.10}$$

5. The residual force is compared to the tolerance set by the user; the default value in BRIGADE/Plus is 0.5 % of the average force in the system. The last displacement correction used is compared to its tolerance, which is by default 1 % of the total displacement incrementation Δu_{i+1}, where $\Delta u_{i+1} = u_0 - u_{i+1}$.
6. If both R_{i+1} and c_{i+1} is within the tolerances the configuration is considered to be in equilibrium with the load and a new increment can start with a new ΔP as the load increment. If the system is not considered to be in equilibrium using the tolerances specified a new iteration will take place starting from the configuration, u_{i+1}, obtained in the first iteration.
7. A new tangent stiffness K_{i+1} is calculated and the process starts over from the beginning as long as the residual force and the displacement correction lies outside its respective tolerances.

Each iteration results in a configuration which is closer the true equilibrium solution u_b corresponding to the load P_b. (Simulia, 2009a), (Simulia, 2009b)

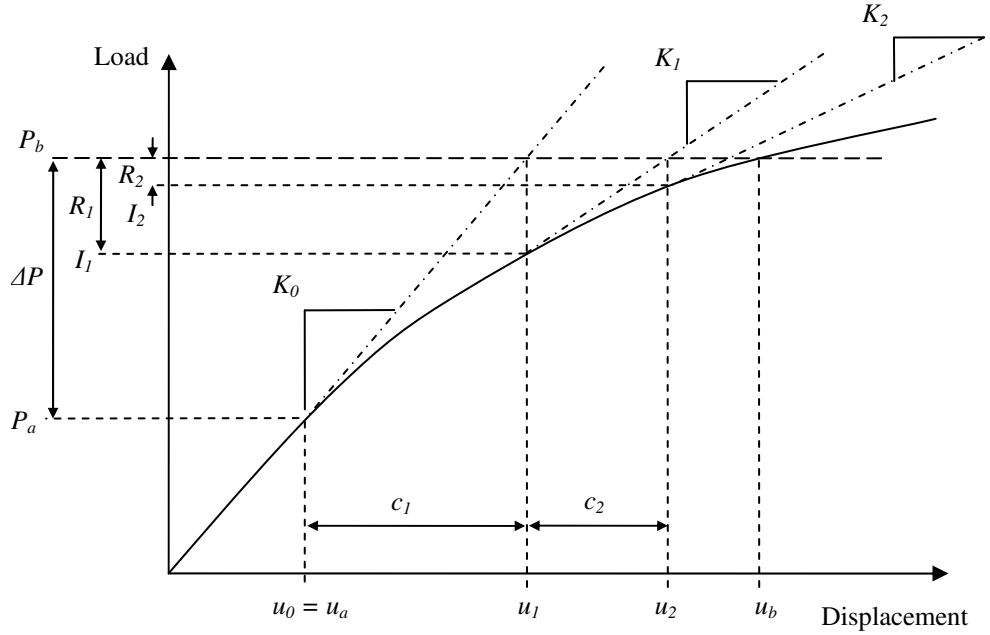

Figure 4.12 Schematic representation of how Newton's method solves non-linear problems. Adapted from Simulia (2009a).

5 FE-analysis of bridge 16-935-1

In order to find out what have caused the cracks of the bridges mentioned in chapter 2, a FE-model of one of the bridges was generated and a number of analyses with different loads and material parameters were performed. This chapter describes how the model was generated and what the results from the analyses were. The bridge chosen for the case study was the bridge at junction Axevalla, 16-935-1, see section 2.1. It was chosen because it has a geometry that is quite simple to model and because the cracks that have appeared are well documented.

5.1 Model description

The FE-models was generated in the finite element program BRIGADE/Plus. To be able to include the effect of post-tensioning in BRIGADE/Plus and to describe the behaviour of the bridge in a realistic way, a 3D-model was defined for the case study bridge.

5.1.1 Analysis procedures

Three different analyses were performed, two linear analyses, with linear material models and without reinforcement, and one non-linear analysis with non-linear material models and including the reinforcement. In one of the linear analyses the bridge was loaded with the self-weight only and in the other analysis the bridge was loaded first with prestress and then with the self-weight. In the non-linear analysis, the bridge was loaded with both prestress and self-weight, with the load applied as described in section 5.1.9. The results from the analyses are presented in section 5.3.

5.1.2 Geometry

Since the bridge is symmetric about its mid-section, and the load cases studied were symmetric too, only half the bridge needed to be included in the model. The bridge was divided into four different parts in order to be able to define different element and material properties for different parts of the model in a practical way. This way it was also possible to use different FE mesh density in the different parts without having to specify mesh transition. In the model, also the bearings under the transversal beam were included. A schematic plan of the model is presented in Figure 5.1 and an elevation of the model is presented in Figure 5.2. The global coordinate system was defined as indicated in the Figure 5.1 and 5.2. The x-direction is referred to as longitudinal, the y-direction as vertical and the z-direction as transversal direction.

The geometry used in the model was a simplification of the real geometry. In the model, the bridge was assumed to be straight and horizontal, while the real bridge has a vertical curvature. Edge beams and wing walls were omitted in the model, since these parts were expected to have little effect on the cracking of the transversal beam. However, the difference is small and is not expected to influence the results of interest. The effect of this is further discussed in section 7.1.1.

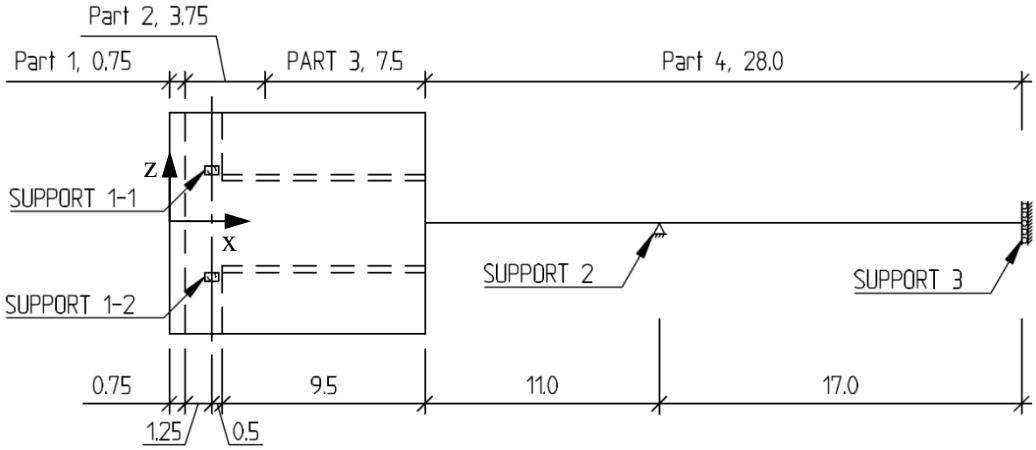

Figure 5.1 Schematic plan of model used for FE-analysis [m].

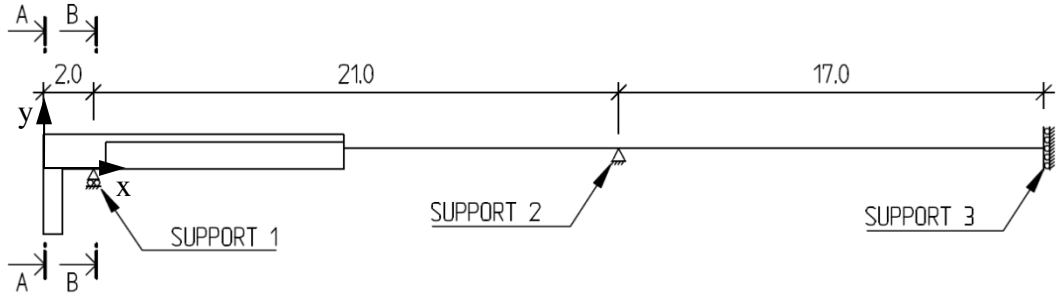

Figure 5.2 Schematic elevation of model used for FE-analysis [m].

Part 1 of the model, see Figure 5.1, consists of the integrated breast wall of the bridge and the dimensions of the cross-section used in the model can be seen in Figure 5.3.

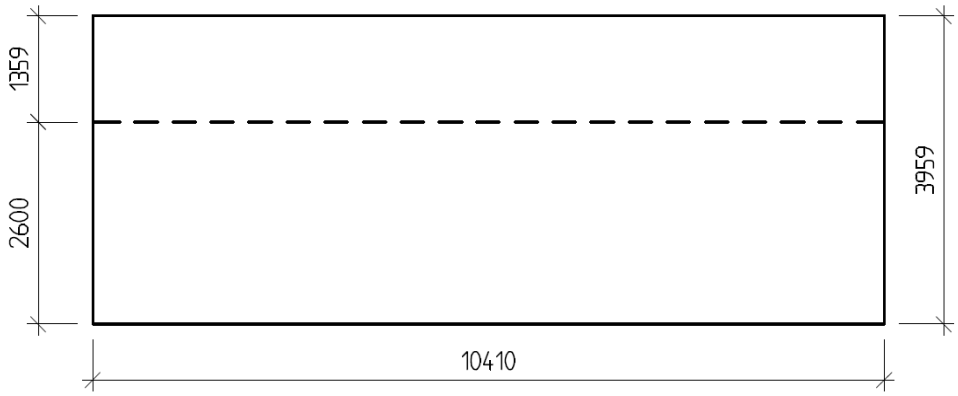

Figure 5.3 Section of the integrated breast wall [mm]. Cross-section A-A according to Figure 5.2.

Part 2 of the model, see Figure 5.1, consists of the transversal beam and 2 meters of the main beam. The geometry of the part, as assumed in the model, is presented in Figure 5.4. The reason to make this part include both the transversal beam and a part of the main beam is that we do not want a constraint in this region, since that might lead to unrealistic stress concentrations.

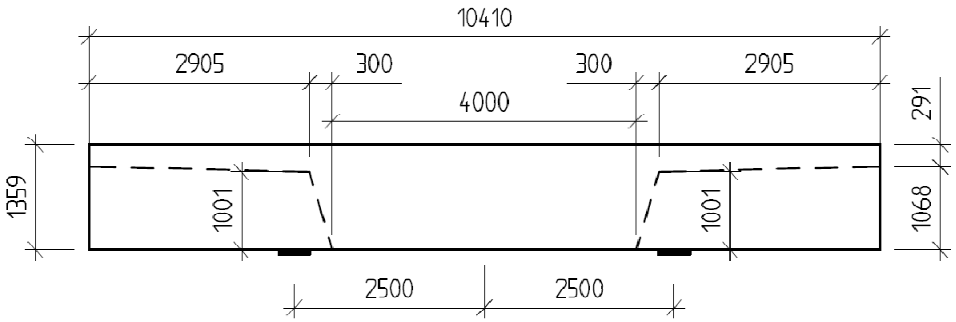

Figure 5.4 Section of main beam (dashed line) and transversal beam (solid line) [mm]. Cross section B-B according to Figure 5.2.

Part 3 is a 7.5 m long part of the main beam, see Figure 5.1 and it has the same cross-sectional shape as the main beam included in part 2, see Figure 5.4.

Part 4 is a 28 m long part of the main beam, see Figure 5.1. Since this part is modelled with beam elements it is not possible in BRIGADE/Plus to draw the sectional geometry. Instead the cross-sectional area and second moment of area in x- and z direction must be specified. These values are calculated using the cross-section of the main beam as shown in Figure 5.4, for part 2.

Support 1-1 and 1-2 are the bearings under the transversal beam, the geometry used in the model can be seen in Figure 5.5. A picture of the generated model is presented in Figure 5.6.

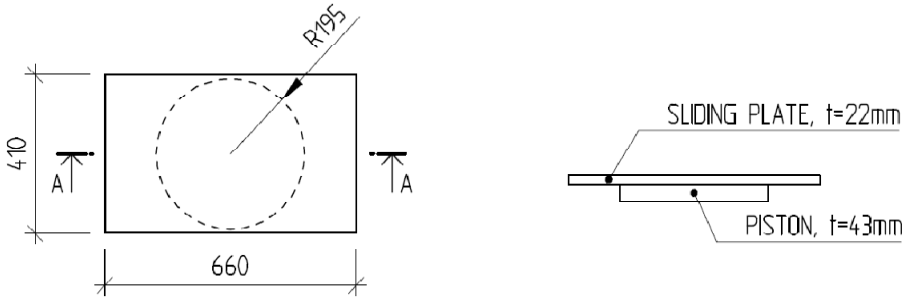

Figure 5.5 Plan of support 1-1 and 1-2, section A-A to the right [mm].

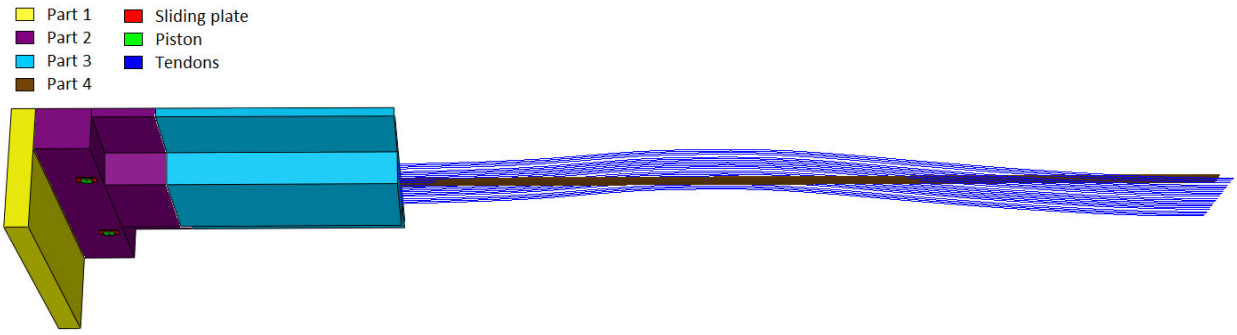

Figure 5.6 Generated FE-model from BRIGADE/Plus, showing the subdivision into different parts.

5.1.3 Reinforcement

The reinforcement is excluded in all parts when a linear analysis is made, since the effect of reinforcement in such an analysis is small. When a non-linear analysis is

performed the reinforcement is included only in part 2 since that is the only part which includes a non-linear material model, see section 5.1.6. Reinforcement is only included in regions where cracking is expected, since it will not have any essential influence before a crack is formed. The reinforcement included in the model is showed in Figure 5.7, Figure 5.8 and Figure 5.9. Note that the reinforcement is only displayed with straight lines, the same way as they are generated in the FE-model. The notations of the included reinforcement are B506, A507, A508, C535, B530 and D531, which are the same as in the original drawings produced by FB Engineering.

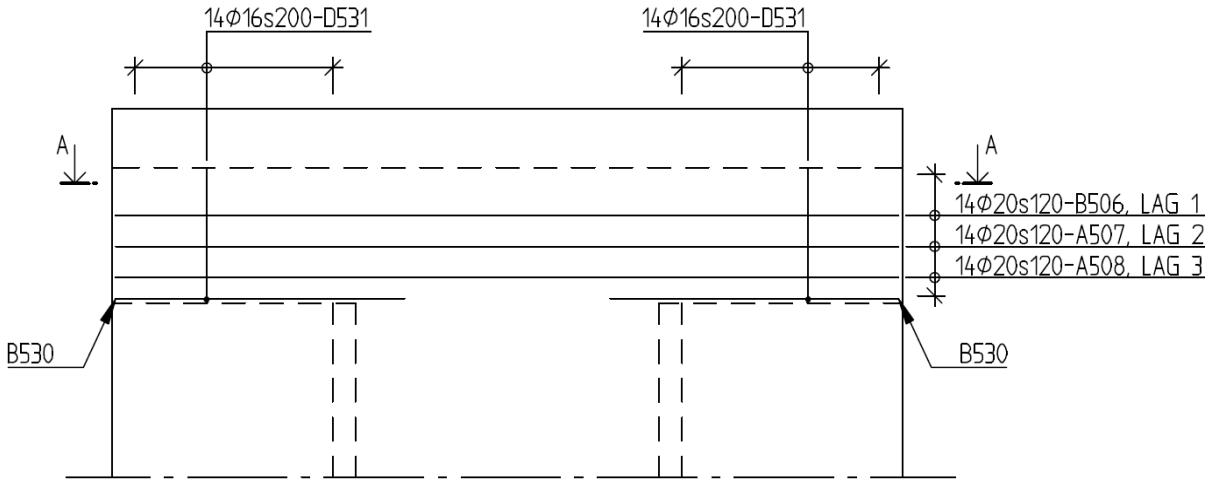

Figure 5.7 Plan of reinforcement arrangement in the FE-model, [mm].

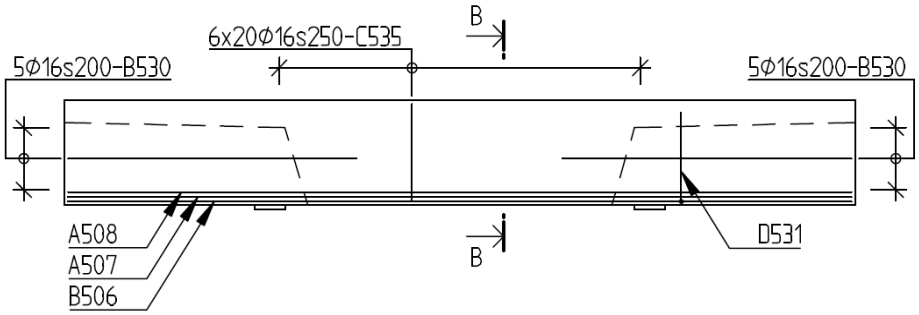

Figure 5.8 Section A-A of reinforcement arrangement in the FE-model, [mm].

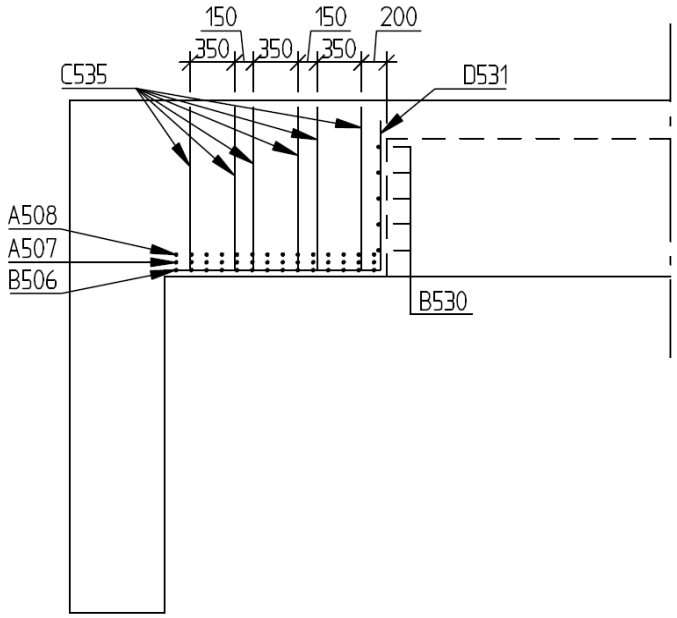

Figure 5.9 Section B-B of reinforcement arrangement in the FE-model, [mm].

5.1.4 Post-tensioning

In the analyses where the post tensioning of the bridge is included, the built in function "Prestress" in BRIGADE/Plus is used. Each tendon is modelled with a cross-sectional area of 0.0018 m^2. The coordinate in x-, y- and z-direction is defined for cross-sections each meter along the bridge and spline functions are used to form the tendons between the coordinates. The tendons are divided into two cable groups which have different positions in the vertical direction; the location of the two cable groups vertical position in the model is presented in Figure 5.10.

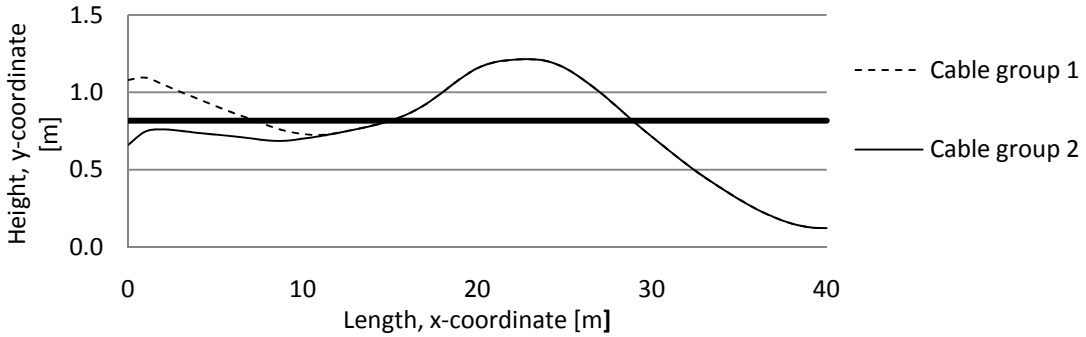

Figure 5.10 Location of cable groups in vertical direction. The height is measured from the bottom of the main beam.

In total there are 24 tendons in the bridge, 12 in each cable group. Cable group 1 consists of tendon 1, 3, 5, 7, 9, 11, 14, 16, 18, 20, 22 and 24 and cable group 2 consists of tendon 2, 4, 6, 8, 10, 12, 13, 15, 17, 19, 21 and 23. The position of each

tendon in the model in the transversal direction is presented in Figure 5.11.

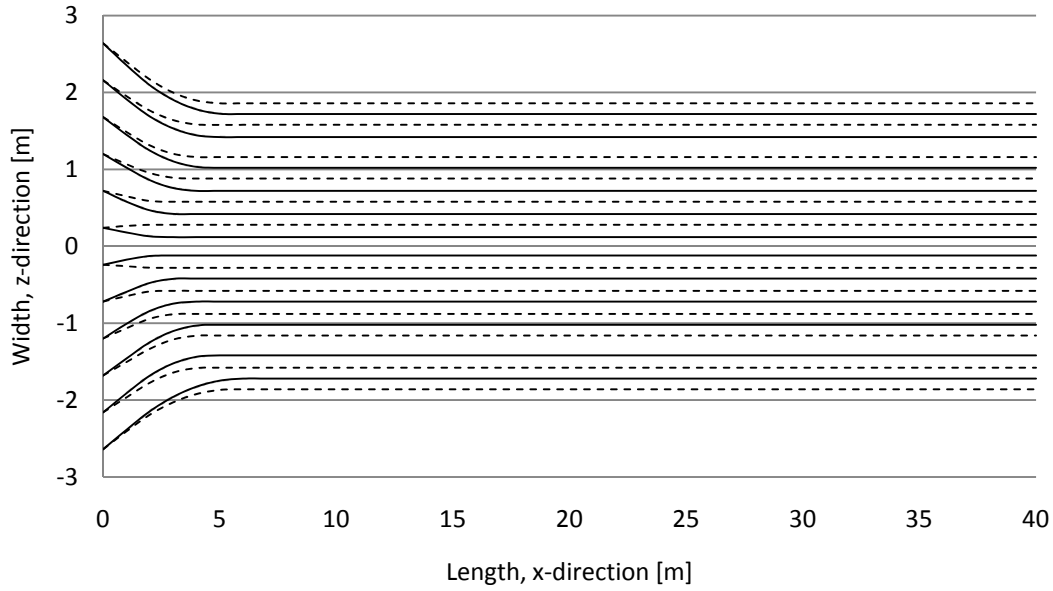

Figure 5.11 Location of tendons in transversal direction. Dashed lines denotes cable group 1 and solid lines denotes cable group 2.

Each tendon is post-tensioned with an initial prestressing force, P_{ini}, of 2367 kN and an allowed force after anchoring of 2230 kN. A friction coefficient μ_f of 0.2 is defined and an unintended angular displacement, k, of 0.0012 m^{-1} is also defined. These values are obtained from the producer of the tendons and recalculated to fit the model for friction loss used in BRIGADE/Plus. (BBR, 2006)

In BRIGADE/Plus it is not possible to define one single tendon along a path through parts with different element types. In order to be able to include the post-tensioning in this model consisting of parts with different element types, a second model must be created to overcome this problem, further referred to as the "tendon model". The "tendon model" is only used to obtain the temperature field along each tendon, as described in section 4.5. This model only consists of one part consisting of beam elements with the same length as the entire original model, functioning as host region for the tendons as described above. A normal static analysis is performed with the "tendon model", which produces a BRIGADE/Plus input data file containing the temperature field that should be applied to each tendon.

Each tendon must now be modelled as two parts in the original model, one part having the solid part of the bridge as host region, and one part having the beam part as host region. The temperature field obtained from the "tendon model" input data file can now manually be inserted into the input data file of the original model, with some modifications due to the fact that each part in the "tendon model" corresponds to two parts in the original model.

5.1.5 Element-types

Four different element types have been used in the model. They are in BRIGADE/Plus called C3D20R and C3D20, which both are solid elements, B31 which is a beam elements and T3D2 which is a truss element. These element types are described more in detail in section 4.2.

The part of most interest, part 2 is model with the solid element type C3D20R at the edges and C3D20 over the bearings and in the centre of the part. The choice of solid elements on this part is that the model should be able to describe cracking that might occur. In order to get the forces to be transferred into part 2 in the most realistic way, part 1 and part 3, the one closest to the part of interest are also modelled with the solid element type C3D20R.

Support 1-1 and 1-2 are modelled with the solid element type C3D20. The decision to use full integration on these parts is that they are so thin so only a couple of elements are placed in height direction.

Part 4 is modelled with the beam element B31. The choice of beam elements on this part is to save computational cost and this part is far away from the part of interest and beam elements should be enough to transfer the sectional forces into the parts modelled with solid elements.

The reinforcement and the prestressing tendons are modelled with truss element type T3D2, since truss elements are the simplest and most efficient way to model reinforcement, see section 4.4 and 4.5.

5.1.6 Material models

The material parameters used were based on the concrete quality (C40/50), reinforcing steel quality (B500 B) and post-tensioning system (CONA CMI 1206-150 1770) specified on the drawings of the bridge. Material parameters corresponding to these qualities were obtained from EN 1992-1-1 (2004).

A number of different material models were used in the 3D-model of the bridge. The elastic material models had different Young´s modulus, E, density, ρ, Poisson´s ratio, ν and thermal expansion coefficient, α_e. The density for concrete includes reinforcement, why the density of reinforcement and prestress is set to 1 kg/m^3. The thermal expansion coefficient for "Prestress" is defined, since it is used to simulate the prestressing force, see section 4.5. The parameters for the different material models are presented in Table 5.1.

Table 5.1 Properties for elastic material models.

Material name	E [GPa]	ρ [kg/m^3]	ν [-]	α_e [1/°C]
Elastic concrete	35	2500	0.2	-
Piston	10^6 (rigid)	7800	0.3	-
Prestress	200	1	0.3	$1.2 \cdot 10^{-5}$
Reinforcement	200	1	0.3	-
Sliding Plate	210	7800	0.3	-

In some of the analyses a non-linear material model was used, the theory of that model is described in section 4.1.3. Here it is referred to as the "Damaged Plasticity" material model. Density, Young´s modulus and Poisson´s ratio are the same as for the "Elastic Concrete" model. But in this model the non-linear behaviour of the concrete and a number of additional parameters should also be defined. The compressive stress

versus plastic-strain behaviour can be seen in Table 5.2, and was calculated according to section 4.1.2. The tensile stress versus crack opening behaviour can be seen in Table 5.3, and was calculated according to section 4.1.1. A bi-linear curve was used based on fracture energy G_f = 115 Nm/m^2. The fracture energy was based on concrete class C40/50 and maximum aggregate size 32 mm. The concrete class was specified on the drawings of the bridge, while the aggregate size was not specified on the drawings. However, the aggregate size should only be specified on the drawings if smaller aggregates than 32 mm are used, which implies that 32 mm aggregates were used in the concrete of the bridge (Vägverket, 2007, section 14.22). Graphs showing the compressive and tensile curves for the concrete are presented in Figure 5.12 and 5.13. Finally five different parameters need to be defined; they are presented in Table 5.4. All these parameters are explained more in detailed in section 4.1, and were chosen to BRIGADE/Plus default values except for the dilation angle which was chosen according to recommendations by Kölfors[3].

Table 5.2 Compressive behaviour used in the "Damaged Plasticity" material model.

σ [MPa]	ε_{pl} [-]
24.00	0
41.12	$3.25 \cdot 10^{-4}$
46.19	$5.80 \cdot 10^{-4}$
48.00	$9.29 \cdot 10^{-4}$
45.98	$1.29 \cdot 10^{-3}$
39.43	$1.97 \cdot 10^{-3}$
27.46	$2.72 \cdot 10^{-3}$

Table 5.3 Tensile behaviour used in the "Damaged Plasticity" material model.

σ [MPa]	w [m]
3.50	0
1.17	$2.63 \cdot 10^{-5}$
$3.5 \cdot 10^{-2}$	$1.18 \cdot 10^{-4}$

[3] Johan Kölfors, Scanscot Technology, 2010-02-17

Table 5.4 Parameters used in the "Damaged Plasticity" material model.

Dilation angel, ψ [°]	Eccentricity, ε	σ_{b0}/σ_{c0}	K_c	Viscosity parameter, μ
35	0.1	1.16	0.67	0

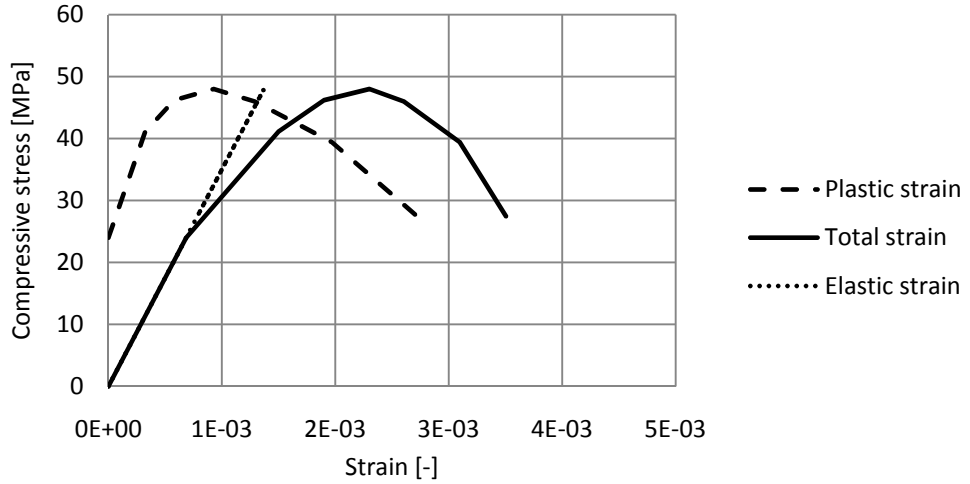

Figure 5.12 Compressive stress versus strain relationship used in the "Damaged placticity" material model.

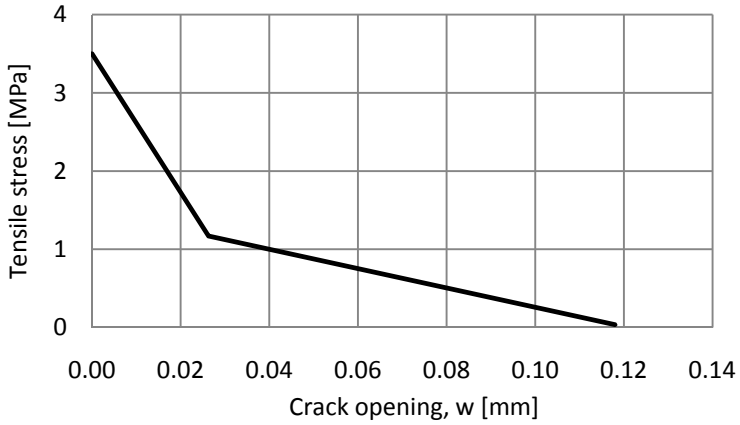

Figure 5.13 Tensile stress versus crack opening relationship used in the "Damaged placticity" material model.

Part 1, the integrated breast wall, is modelled with the "Elastic concrete" material model. An elastic material model is needed for this part since the prestressing forces will give cause to concentrated stresses larger than the tensile strength of the concrete, so the concrete would crack if a plastic material model was used. This would not describe the real behaviour since there are anchorage devices placed in the integrated breast wall in reality. These anchorage devices will spread the anchorage forces but they are not included in the model.

Part 3 and part 4 are modelled with the "Elastic concrete" material model in order to save computational time. No major cracking is expected to occur here, and secondary cracking in those parts are not of interest in our analysis.

The reinforcement is modelled with the "Reinforcement" material model, and the post-tensioning tendons are modelled with the "Prestress" material model.

The bearings under the transversal beam, see Figure 5.5, are modelled with two different material models. The sliding plate uses the "Sliding plate" material model, which is an elastic material model with steel properties and the pistons uses the "Piston" model which is a very rigid material. The choice of a rigid material is because the boundary condition is only applied in one node, to be able to let the bearings rotate. If a non-rigid material model would be used the concentrated forces that occur in this node would make the piston deform in a very unrealistic way.

Part 2, the part of most interest, has different material models in different analyses. When a linear analysis is performed the "Elastic concrete" model is used and when a non-linear analysis is performed the "Damaged Plasticity" material model is used.

5.1.7 Constraints

The interaction between the four parts defined in Figure 5.1 was modelled with the "surface to surface" tie constraint described in section 4.3. Constraints of the same type were also used between the sliding plate and the transversal beam and between the piston and the sliding plate. The constraint between the reinforcement and the concrete was modelled using "embedded elements" constraints. The interaction between the post-tensioning tendons and the solid elements were modelled with "embedded elements" constraints and the interaction between the tendons and the beam elements were modelled with the "surface-to-surface" tie constraints.

5.1.8 Boundary conditions

The position of the supports used in the 3D-model can be seen in Figure 5.1 and Figure 5.4. The boundary conditions are the same as the ones used in the design of the bridge, see Figure 2.3. The boundary conditions for support 1-1 and 1-2 is placed in one point centred at the bottom of each piston. This is because the bearings should be able to rotate and follow the movement of the transversal beam. These supports are fixed in both transversal and vertical direction. Support 2 is fixed in transversal, vertical and longitudinal direction. Support 3 acts as a symmetry line since only half the bridge is included in the model. All the rotational degrees of freedom are fixed and the translation degrees of freedom are fixed in the length direction of the bridge but the support is free to move in transversal and vertical direction.

5.1.9 Loads

Since the cracks in the bridge has appeared before it was loaded by traffic the only loads that are included in the analysis was the self-weight and the post-tensioning.

In the analyses where the self-weight was acting, a gravity load on the whole model was applied with a gravity constant, g, set to be 9.82 m/s^2. In the linear analysis when both post-tensioning and self-weight were applied, the post-tensioning was applied first and the gravity load was applied afterwards.

In the non-linear analysis the post-tensioning was applied simultaneously with half of the self-weight. This was in order to describe the reality in a good way. When the post-tensioning starts to act, the bridge will deflect upwards from the scaffolding and, consequently, a part of the self-weight will be applied to the structure. How much of the total self-weight that is actually applied is hard to estimate, but 50 % was judged

to be a realistic assumption. After the post-tensioning and half of the self-weight was applied the rest of the self-weight was applied on the structure.

When applying the load in the analyses, the step type STATIC GENERAL was used. A load controlled incrementation scheme using automatic incrementation was used for applying the load. The largest increment allowed was set to 5 % of the total load in the current step. The largest increment allowed was specified to get a sufficiently accurate answer regarding when the first crack occurs, and to avoid numerical convergence problems. The Newton iteration method, see section 4.6, was used for solving the equilibrium conditions since it has a fast convergence rate compared to other methods in BRIGADE/Plus. (Simulia, 2009b)

5.2 Verification of the model

Verification was made to see if the model gives a correct result that describes the reality. A global analysis was made to see if the deformations, moments and reaction forces are the same in the FE-analysis as in other analytical calculations. To calculate variables which could be compared with the ones obtained from the FE-analysis the program STRIP STEP2 was used. Furthermore hand calculations of the moment distribution along the beam and the reaction forces were performed using MathCAD.

In STRIP STEP2 a 2D-model of the complete bridge was generated. The model had constant cross-sectional area and second moment of area along the bridge. These constants were calculated using the cross-section of the main beam that was used in the FE-model. The density of the concrete and the gravitational constant was specified and they were the same as those defined in the FE-model. The post-tensioning was defined using the location of the two cable groups in vertical direction and the cross-sectional area was defined as the area of one cable multiplied with the number of cables in each cable group. The model had the same boundary conditions as the FE-model with the exception that the entire bridge length was model, i.e. no symmetry boundary condition was generated and no DOFs existed in transversal direction since the STRIP STEP2 model was made in 2D.

The hand calculations can be followed in Appendix A1, and the STRIP STEP input file is shown in Appendix B.

For the verification, the FE-model described in section 5.1 with the “elastic concrete” material model in part 2, as described in section 5.1.6, was used.

5.2.1 Verification of global behaviour due to self-weight

To verify if the mesh was fine enough to yield an accurate result on the global scale, a convergence study was made. The mesh was refined simultaneously on the parts modelled with solid elements and the part modelled with beam elements. The bridge was only loaded with self-weight. The moment distribution, deflection and reaction forces were also compared with the results from STRIP STEP2 and the moment distribution and reaction forces were also compared with hand calculations.

In the first analysis an approximate mesh size of 0.3 m on the solid parts and 1.0 m on the beam part were chosen and in the second analysis an approximate mesh size of 0.15 m on the solid parts and 0.5 m on the beam part were chosen. The results of the moment distribution and the deflection can be seen in Figure 5.14 and Figure 5.15. The reaction forces at supports are presented in Table 5.5.

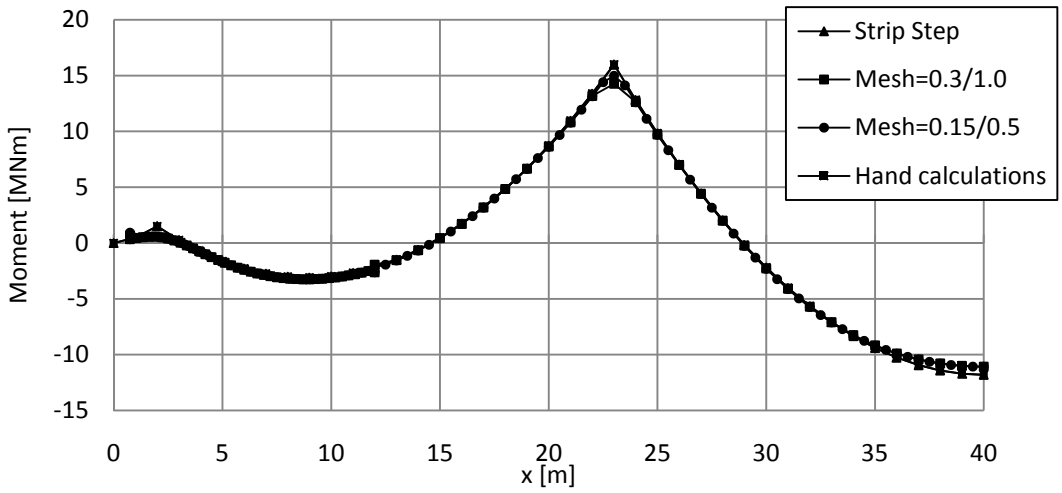

Figure 5.14 Moment distribution due to self-weight along the model.

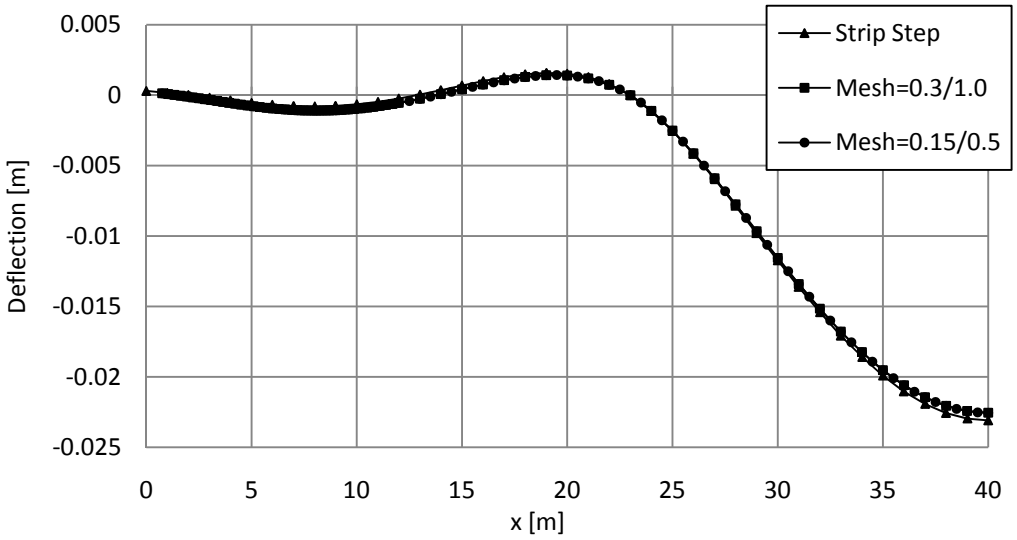

Figure 5.15 Deflection due to self-weight along the model.

Table 5.5 Reaction forces at supports due to self-weight.

Support	Brigade, Mesh = 0.3/1.0 [kN]	Brigade, Mesh = 0.15/0.5 [kN]	Strip Step [kN]	Hand calculations [kN]
1	2601.16	2600.58	2523.43	2523
2	5981.60	5982.19	5980.35	5981
Total	8582.76	8582.77	8503.78	8504

The total load applied in the FE-model was 8582.765 kN, which corresponded well to the reaction forces obtained in the model.

Since the results obtained from analyses made with both meshes are very close to the results obtained from STRIP STEP2 and hand calculations it is reasonable to assume that that a mesh size of 0.3 m on the solid parts and 1.0 m on the beam part should be enough to describe the global behaviour of the bridge due to self-weight.

5.2.2 Verification of global behaviour due to prestress

To verify if the post tensioning forces is defined properly in BRIGADE/Plus an analysis of the bridge loaded only by the post-tensioning was performed with the mesh chosen based on results presented in the previous section. In order to obtain the moment distribution along the solid parts (which only provides output in terms of stresses) the stresses in the centre of the bottom face of the solid parts were collected. The stresses along the two tendons situated closest to the centre, one for each cable group, were as well collected. From these stresses the forces in each cable group were calculated using Equation 5.1, assuming that the 12 tendons in each cable group had the same force distribution.

$$P_i(x) = \sigma_t(x) \cdot A_t \cdot 12 \tag{5.1}$$

Where

$P_i(x)$ is the force in cable group i, at length coordinate x.

$\sigma_t(x)$ is the stress in one tendon, at length coordinate x.

A_t is the cross-sectional area of one tendon.

x is the length coordinate as defined in Figure 5.1.

The bending moment in the corresponding nodes could then be calculated according to the following expression:

$$M(x) = -(\sigma_{le} + \frac{P_1(x) + P_2(x)}{A_c}) \cdot \frac{I_b}{z_{le}} \tag{5.2}$$

where

$M(x)$ is the bending moment at length coordinate x.

$\sigma_{le}(x)$ is the concrete stress at the centre of the bottom face of the solid part, at length coordinate x.

A_c is the cross-sectional area of the main beam.

I_b is the moment of inertia of the main beam.

z_{GC} is distance from the bottom of the beam to the centre of gravity.

$P_1(x)$ is the force in cable group 1, calculated according to Equation 5.1.

$P_2(x)$ is the force in cable group 2, calculated according to Equation 5.1.

The moment distribution obtained in BRIGADE/Plus, for the case when prestress is applied, together with the corresponding moment distribution obtained from STRIP STEP2 can be seen in Figure 5.16.

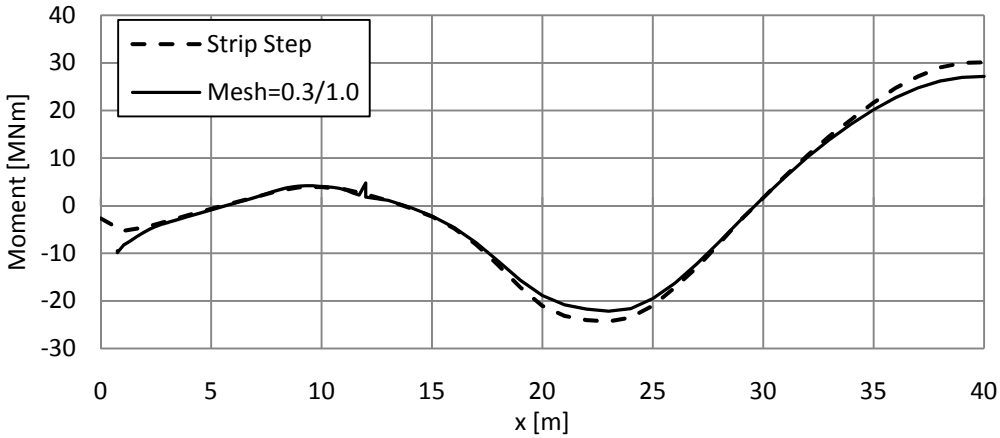

Figure 5.16 Moment distribution due to prestress.

The result obtained from BRIGADE/Plus differs from that obtained in STRIP STEP2 with a maximum magnitude of about 10 %. The difference is due to two reasons:

- BRIGADE/Plus applies a prescribed strain to the tendons which corresponds to the initial prestressing force. When the prestress is applied, the concrete will be compressed and the tendons will be elongated in order to fulfil strain compatibility. Consequently the strain in the tendons will be less than the prescribed strain, corresponding to a force less than the initial prestressing force, see Figure 5.17. STRIP STEP2 does not account for this effect.[4]

- BRIGADE/Plus accounts for friction losses due to curvature of the tendons in transversal direction, see Figure 5.11, which is not accounted for in STRIP STEP2.

This indicates that STRIP STEP2 overestimates the effect of the prestressing force, and the most credible results are the ones obtained in BRIGADE/Plus. The model can therefore be assumed to describe the global response due to prestress in an appropriate manner.

[4] Johan Kölfors, Scanscot Technology, 2010-02-17

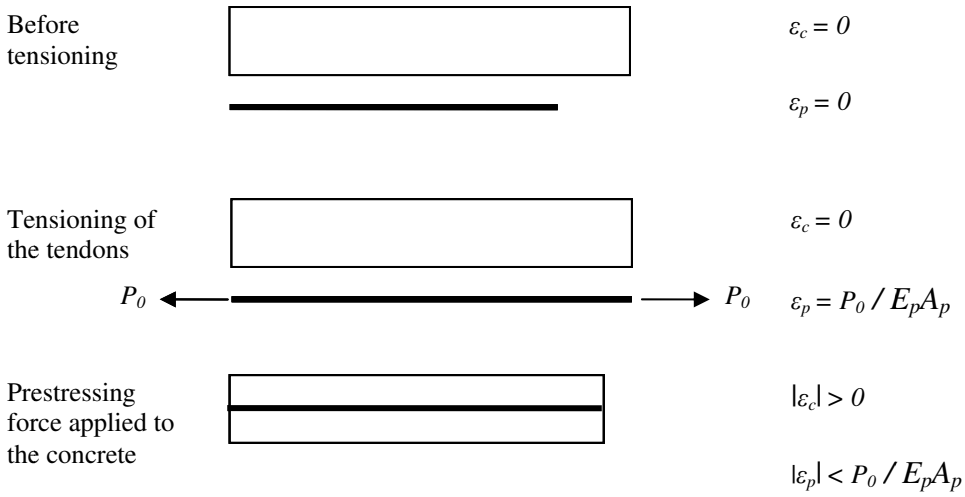

Figure 5.17 Explanation to how BRIGADE/Plus apply the prestressing force.

5.2.3 Verification of local behaviour due to self-weight and prestress

The results presented above shows that the FE model gives trustworthy results on a global scale. In order to verify that the model also gives credible result for the local response, a convergence study regarding the finite element size was made. The maximum principal stresses on the transversal beam are presented in Figure 5.18 for a mesh size of approximately 0.3 m and in Figure 5.19 for a mesh size of 0.15 m.

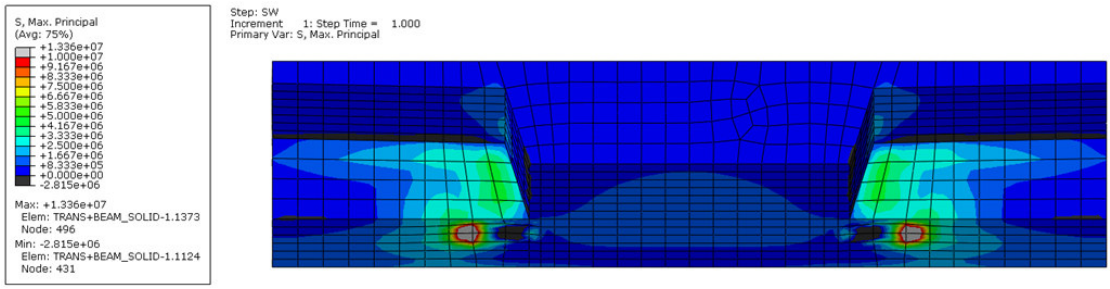

Figure 5.18 Maximum principal stresses due to self-weight and prestress, mesh size approximately 0.3 m.

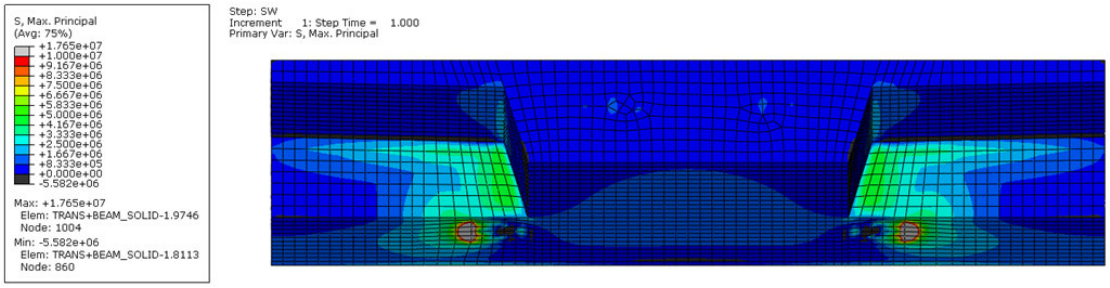

Figure 5.19 Maximum principal stresses due to self-weight and prestress, mesh size approximately 0.15 m.

The figures above show that the stress field was very similar irrespectively of if the finer or the more coarse mesh was used. The only exception is that the maximum stress value of the finer mesh is higher than in the coarser mesh. However, the maximum value is in the region above the bearing where unrealistic stress concentrations are likely to occur. It is a known problem that concentrated stresses increases as the mesh is refined, due to the fact that the same force might act in one node, but the "area" connected to this node is reduced with reduced mesh size and, consequently, higher stresses occur.

In order to be able to obtain a crack pattern with reasonable accuracy, the finer mesh of 0.15 m was used in all subsequent analyses, both linear and non-linear.

5.3 Results from FE-analysis

In this chapter results from the three different analyses are presented. In the elastic analyses the maximum principal stresses are presented to see if it is likely that cracking will occur. In these results positive stresses are tensile stresses and negative stresses are compressive stresses. In the non-linear analysis the tensile equivalent plastic strain is presented in order to see if cracks have formed. The deformed shape of the transversal beam is also presented when both prestress and self-weight is applied. For both linear and non-linear analyses the reaction forces at the bearings under the transversal beam is presented.

5.3.1 Linear model with self-weight

When the self-weight was added small compressive stresses occur in the areas where the bearings are positioned and tensile stresses are situated around them. The reaction forces for the bearings in transversal and vertical direction are presented in Table 5.6 where V1 and V2 are the vertical reaction forces for bearing 1-1 and 1-2 respectively and T1 and T2 and the transversal reaction forces for bearing 1-1 and 1-2 respectively. The results from the analysis show that when only the self-weight is applied there is no risk of cracking since the maximum principal stresses is much smaller than the mean tensile strength of the concrete, see Figure 5.20.

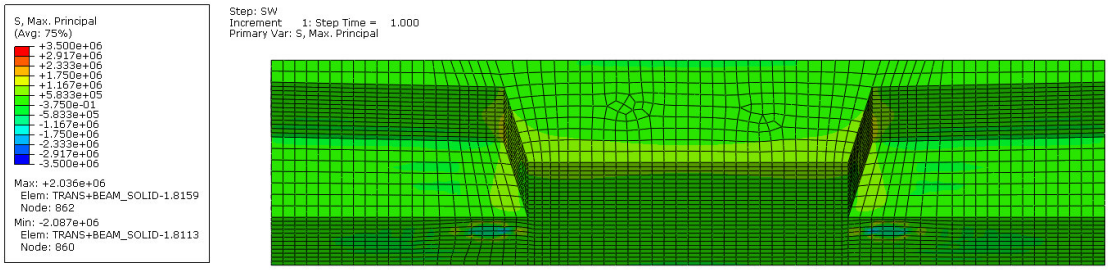

Figure 5.20 Maximum principal stresses due to self-weight.

Table 5.6 Reaction forces at bearings in vertical (V1, V2) and transversal (T1, T2) direction.

	V1 [kN]	V2 [kN]	T1 [kN]	T2 [kN]
Self-weight	1320	1320	183	-183

5.3.2 Linear model with self-weight and prestress

When the prestress was applied tensile stresses which are larger than the mean tensile strength of the concrete appears around the bearings and in at the front surface of the transversal beam. This shows that there is a large probability for the beam to crack. Figure 5.21 shows the principal stresses of the transversal beam, where the grey areas had maximum principal stresses larger than the mean tensile strength of the concrete.

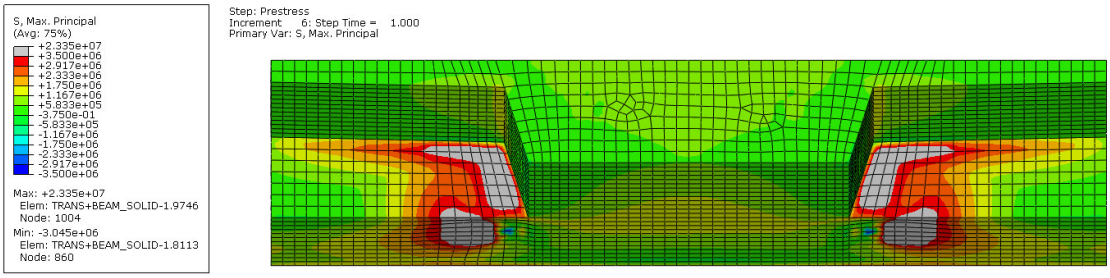

Figure 5.21 Maximum principal stresses due to prestress.

When the self-weight was added the maximum principal stress distribution changed, see Figure 5.22. Compressive stresses appeared, the regions marked with blue, and the tensile stresses on the front face of the transversal beam were redistributed and concentrated closer to the main beam.

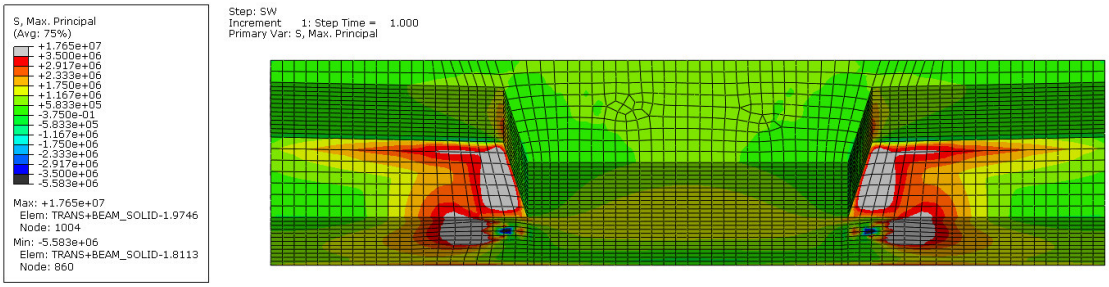

Figure 5.22 Maximum principal stresses due to prestress and self-weight.

The reaction forces at the bearings for both load cases in this analysis are presented in Table 5.7. These results show that the bottom of the transversal beam wants to be elongated in transversal direction due to the prestressing force, but the displacement was prevented by the bearings which are fixed in transversal direction.

Table 5.7 Reaction forces at bearings in vertical (V1, V2) and transversal (T1, T2) direction due to prestress and self-weight.

	V1 [kN]	V2 [kN]	T1 [kN]	T2 [kN]
Prestress	79.9	79.4	2090	-2090
Prestress + self-weight	1400	1400	2270	-2270

5.3.3 Non-linear model with self-weight and prestress

When the non-linear material model is used, BRIGADE/Plus calculates the tensile equivalent plastic strain, $\varepsilon_{pl,t}$. In areas where $\varepsilon_{pl,t}$ is larger than zero cracking of the concrete has occurred due to tensile stresses. Cracking started at the end of the both bearings, when 19 % of the prestress and 9.5 % of the self-weight was added, see Figure 5.23.

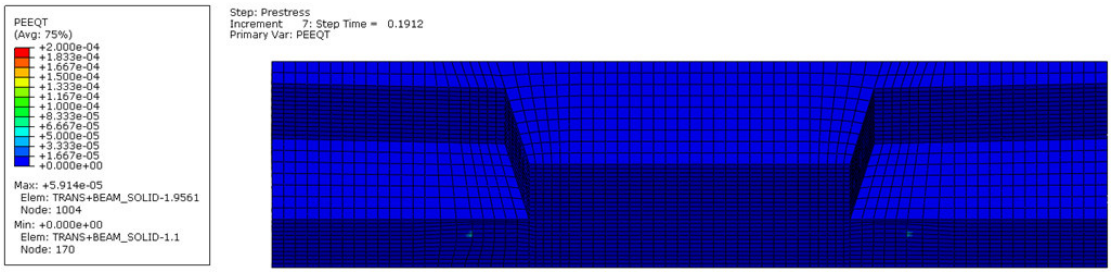

Figure 5.23 Tensile equivalent plastic strain when first crack appears.

The cracks propagated towards the front face of the transversal beam and reached the front face when 79 % of the prestress and 39.5 % of the self-weight was added. The tensile equivalent plastic strain when all of the prestress and half of the self-weight were applied is showed in Figure 5.24. When the rest of self-weight was added, the strain increases slightly in the cracked elements closest to the main beam, see Figure 5.25.

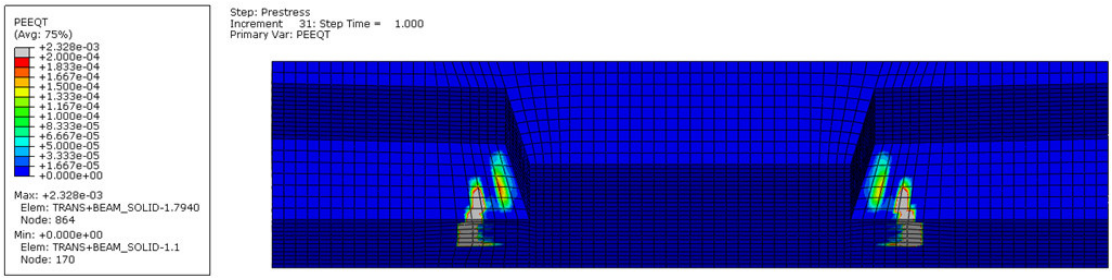

Figure 5.24 Tensile equivalent plastic strain due to prestress and half the self-weight.

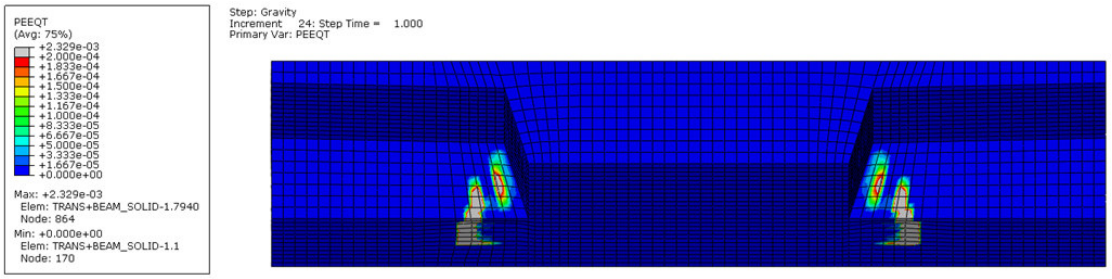

Figure 5.25 Tensile equivalent plastic strain due to prestress and self-weight.

Figure 5.26 shows the deformed shape of the transversal beam when both prestress and self-weight were applied. The red line in the figure indicates the initially straight line along the front of the transversal beam, which became distorted due to the prestressing force. The main beam was compressed uniformly by the prestressing force, creating the straight part of the red line in the centre of Figure 5.26. The ends of

the transversal beam and the cantilevering slab of the superstructure were however not stressed by compressive stresses, since the prestressing force was not yet distributed uniformly over the entire cross-section, see Figure 5.27. Consequently, the ends of the transversal beam were prevented by the cantilevering slab to shift longitudinally together with the main beam, causing the bend of the red line.

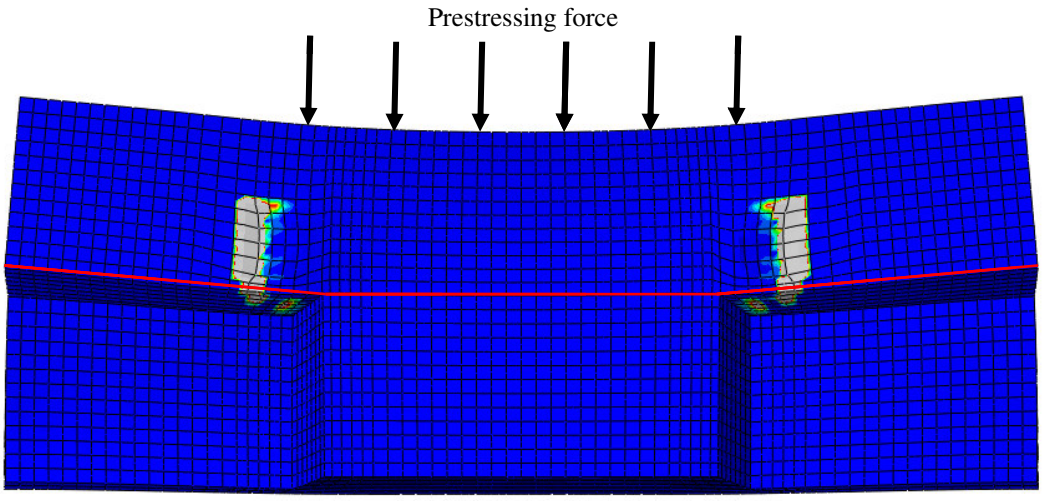

Figure 5.26 Deformation of the transversal beam due to prestress and self-weight, deformation scale factor 500.

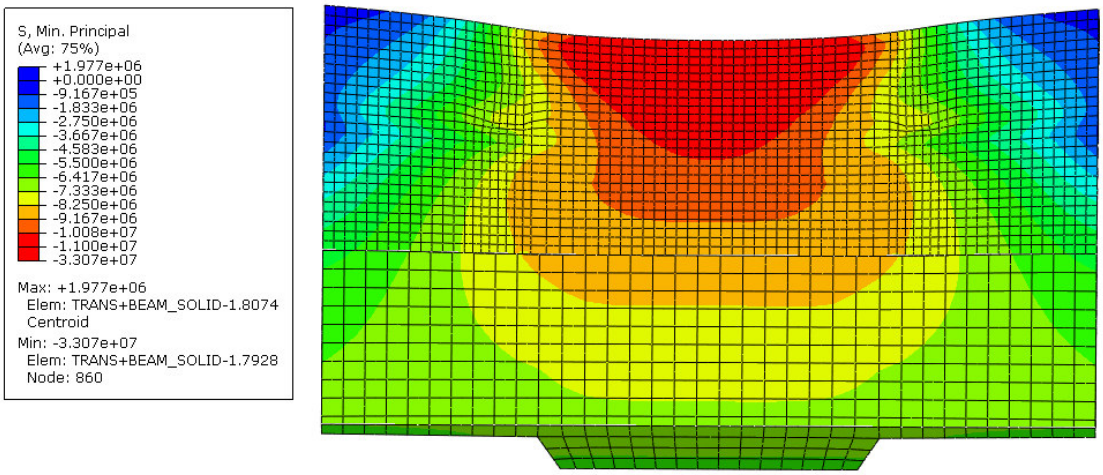

Figure 5.27 Minimum principal stresses (i.e max compressive stress) due to prestress and self-weight seen from above.

The reaction forces at the bearings when the prestress and the self-weight were added are presented in Table 5.8. The reaction forces for the total load are slightly smaller than the ones obtained in the elastic analysis see Table 5.7, this is because that the cracking have weakened the transversal beam which has lead to a small redistribution of the reaction forces.

Table 5.8 Reaction forces at bearings in vertical (V1, V2) and transversal (T1, T2) direction due to prestress and self-weight.

	V1 [kN]	V2 [kN]	T1 [kN]	T2 [kN]
Prestress+0.5· Self-weight	715	715	1500	-1500
Prestress + Self-weight	1370	1370	1590	-1590

6 Parametric study

In order to see what measures that can be taken to prevent the cracking, additional analyses were made. The models used in the following analysis are the model described in chapter 5 with changes that are described in each of the following chapters. When a linear analysis was performed the only result presented is the maximum principal stresses in the transversal beam when the self-weight and the prestress is applied. When a non-linear analysis was performed the only result presented is the tensile equivalent plastic strain in the transversal beam when the self-weight and the prestress are applied.

The following changes were made to the model and analyses were made for each change.

- Releasing one of the bearings degree of freedom in transversal direction.
- Adding additional horizontal reinforcement in the front face of the transversal beam.
- Adding additional horizontal reinforcement in the front face of the transversal beam in combination with releasing one of the bearings degree of freedom in transversal direction.
- Increasing the width of the transversal beam in the longitudinal direction.
- Inserting a small wedge between the main and the transversal beam.
- Inserting a large wedge between the main and the transversal beam.

6.1 Free in transversal direction

The change made in the following analyses was that the degree of freedom in transversal direction of bearing 1-1 is no longer fixed. Two analyses were made, one linear analysis with the result presented in chapter 6.1.1 and one non-linear analysis with the result presented in chapter 6.1.2.

6.1.1 Results from linear analysis

When releasing bearing 1-1 in transversal direction the stress distribution became different compared to the results from the elastic analysis in section 5.3.2, where bearing 1-1 was fixed in transversal direction. The critical regions, where the tensile stresses became larger than the concrete tensile strength, were here closer to the main beam and were not starting over the bearings, see Figure 6.1. This shows that if this change was made cracks would still appear, but the cracks would be situated closer to the main beam. This is because no restraint is created between the bearings, and no stress concentrations are caused in this region.

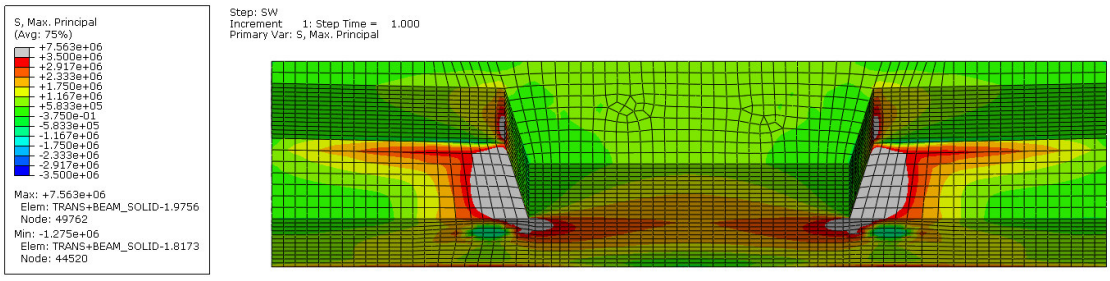

Figure 6.1 Maximum principal stresses due to prestress and self-weight for the linear model with transversal displacements allowed in one bearing.

6.1.2 Results from non-linear analysis

The non-linear analysis showed that the cracks develop closer to the main beam, as expected based on the elastic analysis presented above. Figure 6.2 shows the tensile equivalent plastic strain when both the prestress and the self-weight are applied. The strains has decreased in comparison with the analysis made with the original boundary conditions, see Figure 5.25.

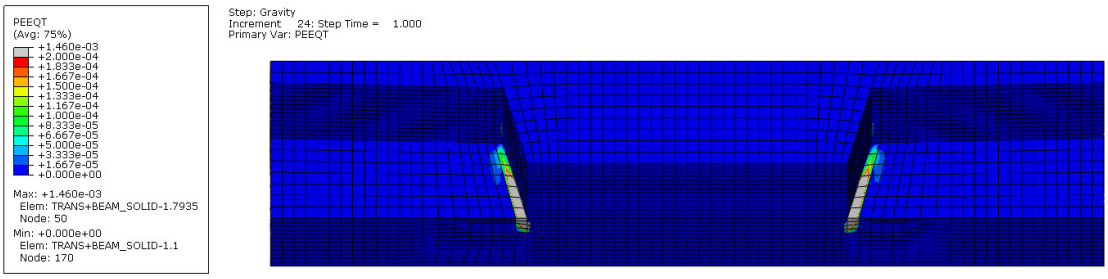

Figure 6.2 Tensile equivalent plastic strain due to prestress and self-weight for the non-linear model with transversal displacements allowed in one bearing.

6.2 Increased horizontal reinforcement amount

In this analysis additional horizontal surface reinforcement in the front face of the transversal beam was inserted in the original non-linear model. The reinforcement with notation B530, see Figure 5.8, was changed. The reinforcement diameter was increased from 16 mm to 20 mm and the spacing was changed from 200 mm to 100 mm which means that five additional bars were inserted over each bearing. This means that the amount of horizontal reinforcement in the front face was approximately 3 times as much as in the original analysis. One analysis with the original boundary conditions and one where the boundary condition of bearing 1-1 was released in transversal direction was performed and they are presented in the two following chapters.

6.2.1 Results with fixed transversal displacements

The tensile equivalent plastic strain at the transversal beam when both the prestress and the self-weight were added is presented in Figure 6.3. The crack pattern are the same as for the original model, see Figure 5.25, but in this analysis the strains has decreased which indicates that the crack width would decrease if additional surface reinforcement was inserted.

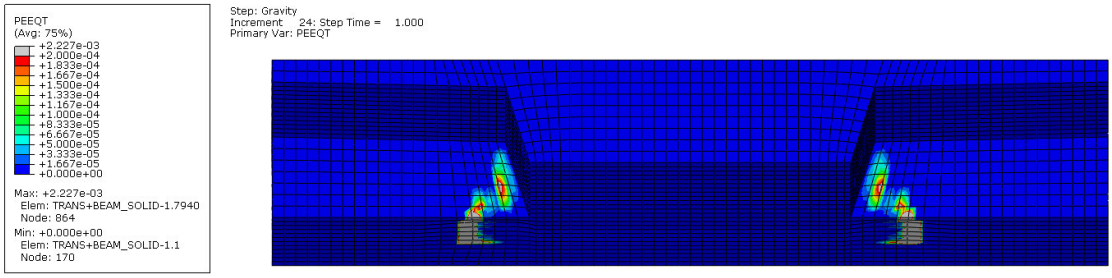

Figure 6.3 Tensile equivalent plastic strain due to prestress and self-weight for the non-linear model with increased horizontal reinforcement amount in the front face of the transversal beam and fixed transversal displacements.

6.2.2 Results with free transversal displacements

When bearing 1-1 was free to move in transversal direction and the prestress and self-weight is added the cracks became located close to the main beam, see Figure 6.4. The strains have decreased significantly in comparison to the analysis where bearing 1-1 was free in transversal direction, but where the original reinforcement amount was used, as described in section 6.1.

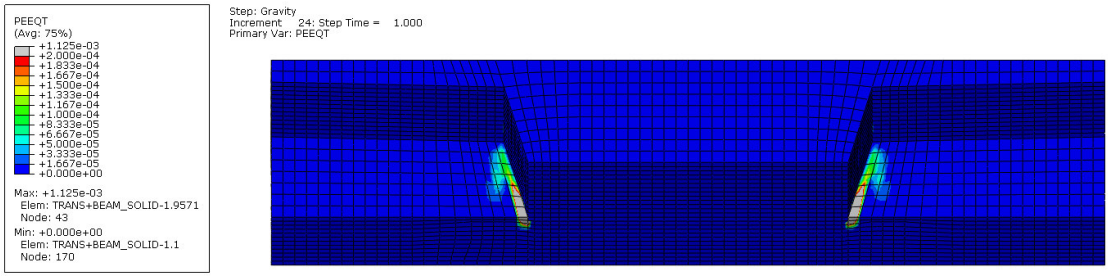

Figure 6.4 Tensile equivalent plastic strain due to prestress and self-weight for the non-linear model with increased horizontal reinforcement amount in the front face of the transversal beam and free transversal displacements.

6.3 Wider transversal beam

The width of the transversal beam was increased with 500 mm in the longitudinal direction of the bridge and a linear FE-analysis was made to see if this measure gives cause to lower stresses.

The maximum principal stresses at the transversal beam when both the prestress and the self-weight were applied are presented in Figure 6.5. It shows that a crack would still occur at the surface but the stresses are slightly smaller than the ones obtained with the original model, see Figure 5.22.

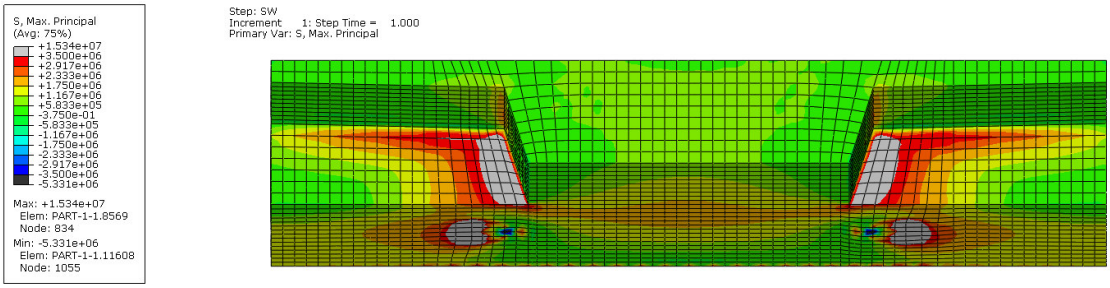

Figure 6.5 Maximum principal stresses due to prestress and self-weight for the linear model with increased width of the transversal beam.

6.4 Small wedge between main and transversal beam

One wedge on each side of the main beam was added to the original linear model. The wedges' dimensions and position are presented in Figure 6.6.

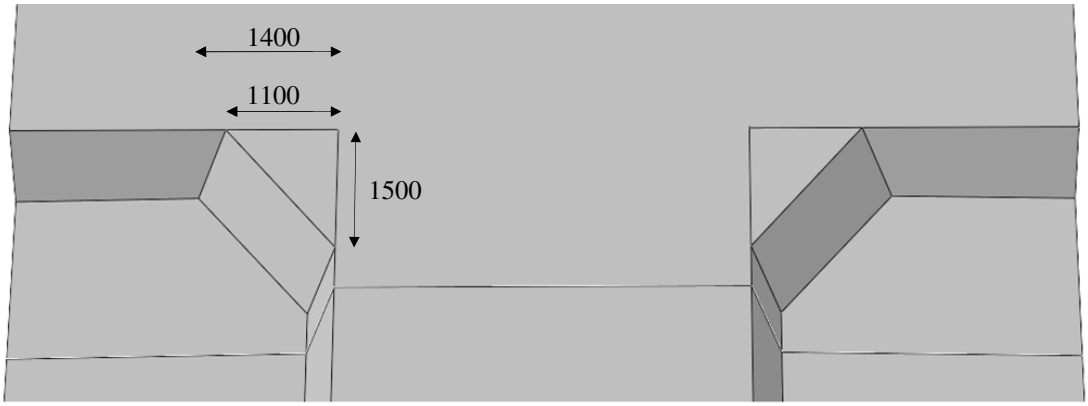

Figure 6.6 Dimensions of the small wedge [mm].

The maximum principal stress field in the transversal beam with both self-weight and prestress applied from a linear FE-analysis is presented in Figure 6.7. The stress concentrations became different in comparison to the linear analysis with the original model, see Figure 5.22. Including a small wedge shows that there is still a large probability that the beam would crack but the crack is probably moved to the region where the wedge meets the transversal beam.

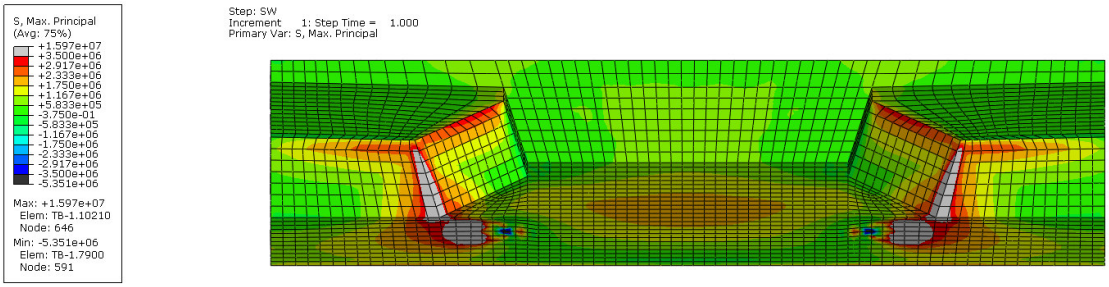

Figure 6.7 Maximum principal stresses due to prestress and self-weight for the linear model with a small wedge inserted.

6.5 Large wedge between main and transversal beam

One larger wedge on each side was added to the original linear model. The wedges' dimensions and position are presented in Figure 6.8.

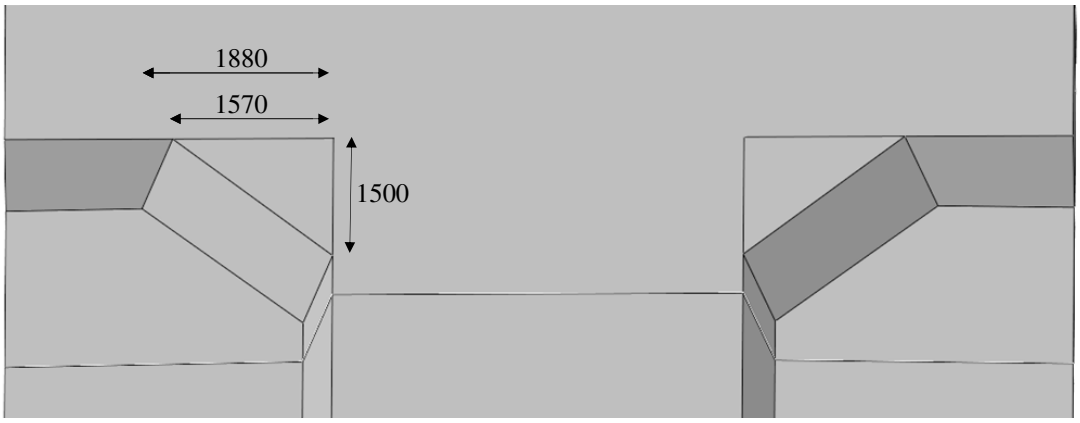

Figure 6.8 Dimensions of the large wedge [mm].

The maximum principal stresses in the transversal beam when both the prestress and the self-weight were applied in a linear FE-analysis are presented in Figure 6.9. Compared to the result obtained from the analysis made with the smaller wedge, see Figure 6.7, the regions where the maximum principal stresses exceeds the tensile strength of the concrete decreases in size.

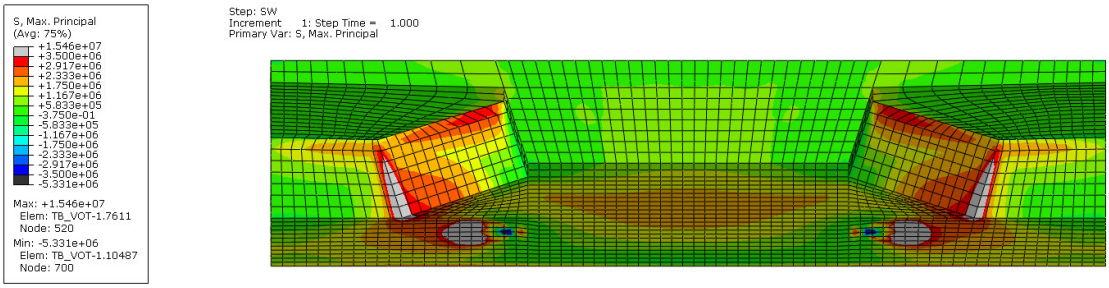

Figure 6.9 Maximum principal stresses due to prestress and self-weight for the linear model with a large wedge inserted.

7 Discussion

7.1 Uncertainties in the FE-model

The analyses presented in chapter 5 and 6 are based on the finite element method, which is a method for solving differential equations numerically. When such an analysis is carried out one must carefully consider the uncertainties and limitations of the analysis, and be aware of that the model might not represent the reality in an exact manner. Limitations and uncertainties of the FE-analyses are discussed in this section.

7.1.1 Geometrical deviations

The FE-model used to simulate the behaviour of the bridge at junction Axevalla, 16-935-1, was only an approximate representation of reality in terms of geometry. The cross-sectional shape of the main beam was less complex than the real one in order to simplify the build-up of the model. Other geometrical simplifications were that wing-walls were not included in the model and that the vertical radius of the bridge was neglected. Our opinion is that none of these simplifications are influencing the outcome of the study significantly, based on the following reasoning:

- The cross sectional shape of the main beam is constant along the bridge, which implies that the sectional forces and moments are not dependent on the stiffness of the beam. The uncertainty is instead linked to the deviation of the vertical load, which will be discussed in section 7.1.2.
- The wing-walls can be neglected since they are not part of the load carrying system for the loads which were treated in the study. The uncertainty is rather a matter of the influence of earth pressure, which is discussed in section 7.1.2.
- The vertical radius of the bridge is large, and the curvature is very small compared to the length of the bridge. Consequently, it can be neglected in the analysis.

7.1.2 Loads and boundary conditions

The load cases accounted for in the analysis of the bridge at junction Axevalla, 16-935-1, were self-weight, prestress and the combination of these. The analysis results showed that the self-weight was not giving cause to tensile stresses close to the tensile strength of concrete. Judging from this, it is not likely that cracking will occur due to any vertical load in the serviceability limit state and, consequently e.g. traffic loads are not included in the model. Other loads such as earth pressure, braking forces, temperature effects and differential settlements of the supports are not of the size or type that is likely to influence the results significantly.

Modelling of boundary conditions in an appropriate way that reflects reality is often a difficult part of setting up a FE-model. The difficulty lies in the fact that a fully fixed boundary condition practically never exists in reality. By introducing boundary conditions such that restraints are introduced in the model one might obtain stress concentrations that are not reflecting the reality in an appropriate way. If both bearings below the transversal beam are fixed in the transversal direction, such restraint will be created. We have therefore chosen to perform most analyses with both fixed and free transversal boundary conditions to be able to study the effect of the restraint. The best guess is probably that the reality lies somewhere between these two modelling choices. It is therefore reasonable that the crack patterns and stress fields in reality also lies somewhere between those obtained from the two modelling choices.

7.1.3 Material parameters and models

The material parameters used in the model were gathered from various studies, where extensive testing and research have been made to quantify the behaviour of concrete. The question is not whether or not these studies are correct; it is rather a matter of if the concrete used in the existing bridge have the properties which were intended. No results from testing of the actual strength have been found from the bridge studied. Instead the material parameters were estimated based on the concrete quality specified on the drawings of the bridge. Mean values of material parameters have been used in the model where such values are available. The difference between values used in the model and the actual real values is however not considered to be of the magnitude that would influence the conclusions in this thesis. It might rather be a question of the size and width of the cracks; an issue that has not been in focus for the study since such estimations in general are very rough.

The material models used in the non-linear FE-model were both elastic and plastic. Elastic models were used in regions where stresses are not assumed to give cause to non-linear deformations. It was shown that this assumption was correct by studying the stress field obtained in these parts. However, concentrated stresses higher than the strength of concrete do occur in the anchorage zone of the prestressing tendons, in a part which is treated as elastic. Our judgement is that the model is still a good representation of the real bridge. These regions are in reality heavily reinforced, and the tendon forces are transferred to the concrete by the tendon anchors, which will allow for the distribution of stresses without any considerable non-linear deformation of the material, influencing the studied response.

The plastic material model for concrete used in this study is able to describe the non-linear behaviour of concrete in both compression and tension. It accounts for the loss of stiffness as the material is strained harder, using a user-defined stress-strain curve for the material. However, this is still only a numerical representation of reality, which will never be equivalent to the real behaviour. Limitations in the model used are mainly that it in principle can not catch the formation and propagation of individual cracks, nor can it with good accuracy describe the size or crack widths of these cracks. For a mesh size which is reasonable with regard to numerical solution problems and computational cost, it will rather give an indication of the crack pattern.

7.2 Comparison with the crack mapping

The cracks patterns obtained in the non-linear analysis carried out with the original design, see Figure 5.25, are similar to the ones that were detected for the real bridge with some exceptions, see the crack mapping in Figure 2.4 and Figure 2.5. From the crack mapping it can be seen that the lower ends of the outer cracks are positioned some distance in over the bearings but in the model the cracks have started on the edge of the bearing. The explanation to that might be that the bearings of the bridge can deform more than the bearings in the FE-model, as discussed in section 7.1.2, so that the maximum stresses, in reality appear at a distance in over the bearings. The stress concentrations in at the edge of the bearings could have caused the cracks to start here in the model. According to the mapping a second crack has also occurred on each side, closer to the main beam. These cracks were not found in the analyses. It is possible that they could have been found if the mesh had been refined very much, but the computational time and numerical problems involved in such an analysis would be too large, as discussed in section 7.1.3.

7.3 Cause of the cracks

The results presented in section 5.3 shows that the most likely reason of the cracks found on the case study bridge is the prestressing force. Both hand calculations and the FE-analysis shows that it is not plausible that vertical forces are causing the cracks. As discussed in section 7.1.2 it is also unlikely that any other loads are having any significant effect in the studied region.

The bridges in Brämhult, 15-1415-1, and in Gulbranna, 13-799-1, exhibit similar crack patterns and have a similar design as the case study bridge. It is therefore likely that the cracking in these bridges has also occurred due to the prestressing force. From our point of view, it is also here unlikely that any other loading of the structure would cause these cracks.

The bridge at junction Nol, 15-1544-1/15-1544-2, has a slightly different crack pattern and the cracks develop from the bearing and up into the cantilevering slab. It is possible that the prestressing force have caused the cracks near the support, but since the geometry of this bridge is rather different from that of the case study bridge, no such conclusion can be drawn with certainty.

7.4 Methods to decrease the risk of cracking

When one of the bearings was free to move in transversal direction, see section 6.1, the crack pattern changed but the values of the equivalent plastic strain were similar. This indicates that removing of the restraint will change the location of the crack but the width of the crack would be of the same magnitude. The inventory made in chapter 2 also shows that bridges without this restraint have been subjected to the same type of cracks.

When increasing the width of the transversal beam in longitudinal direction, see section 6.3, the stress distribution on the front face of the transversal beam is similar to the original model. The maximum values of tensile stresses decreases slightly, but the cracks would still arise and would probably be of almost the same width and length. To give any effect, the transversal beam must be extended much further, an alternative which is probably not economically defendable.

When inserting a wedge the region where stresses from a linear analysis exceed the tensile strength changes from the edge of the bearing to the intersection between the wedge and the main beam. The critical region becomes considerably smaller than in the original model but the maximum stress in the region is slightly higher. This shows that cracking would appear in this region. It is possible that a wedge that reaches further out towards the ends of the transversal beam would produce a slightly better outcome. A wedge has however geometry that is more complicated to construct on the building site, and the reinforcement arrangement and detailing could also cause problems.

When increasing the horizontal reinforcement amount in the front surface of the transversal beam the sizes of the plastic regions decreases slightly and the magnitude of the plastic strain decreases, see section 6.2. This is the easiest and probably the cheapest way to reduce the crack widths. If this measure was taken cracks would still appear but the length and width would decrease. The reinforcement could be designed so that crack widths are limited according to e.g. Bro 2004 – Supplement 2.

8 Conclusions

The bridges treated in this report have experienced cracking in transversal support beams before they were loaded by traffic. The transversal beams have been designed using simple 2D static models, including only loads acting in vertical direction on the transversal beam. The design is made using the load combination which gives the largest vertical force on the transversal beam.

The reason of the cracking was, according to the FE-analyses made, shown to be the prestressing force acting in the longitudinal direction of the bridge; it forces the transversal beam to bend in an unfavourable way as described in section 5.3.3.

Since the cracking is due to forces acting longitudinally, and the common design procedure only accounts for forces acting vertically it is obvious that there is a need of a new design method for transversal beams in post-tensioned bridges.

The studied measures to reduce the risk of cracking have been shown to be successful to varying degrees. Increasing the width of the transversal beam, as described in section 6.3, showed little or no positive effect on the cracks. Adding wedges, see sections 6.4 and 6.5, in the corners between the main beam and the transversal beam indicated some positive effects, in particular when a larger wedge were added. However, cracks would still occur and the widths of these cracks need to be controlled. The best measure that could be taken is probably to increase the horizontal reinforcement amount in the front surface of the transversal beam, as described in section 6.2. This is both economically viable and it is providing a guaranteed reduction of the crack widths.

9 Further studies

Since this thesis only includes a detailed study of one bridge, similar FE-analyses of different bridges would improve the basis for general recommendation of how to deal with the problem described. In such a study it would be possible to identify which magnitude of post-tensioning, in combination with different geometrical designs that produce this problem.

There is a need for a new design procedure of transversal beams in post-tensioned bridges taking the prestressing force into account. A simple static model where the prestressing forces are included could be developed. A suggestion of how such a simple model could look is presented in Figure 9.1. The transversal beam could be treated as a beam on elastic foundations. The response of the beam are based on the prestressing force, P, and the relative stiffness of the main beam, k_{mb}, the cantilevering bridge deck, k_{bd}, and the transversal beam EI_{tb}. Control of crack widths can then be performed on the beam. The issue is to quantify the stiffness parameters used in the static model. This could be done by calibration of the stiffness parameters using several FE-models with different geometry.

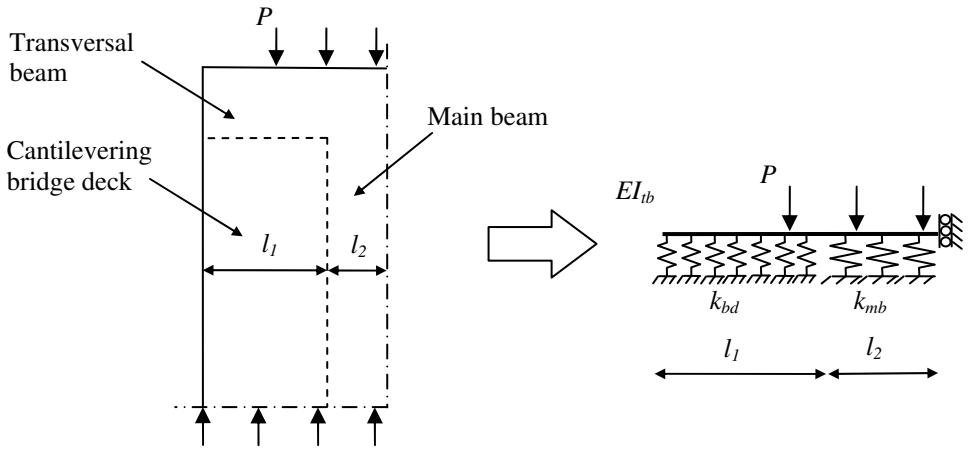

Figure 9.1 Possible static model of the problem studied, which can be used in design.

10 References

Batman (2010): *Bridge and tunnel management (In Swedish)*, Vägverket, (Electronic), Available: <http://www.batman.vv.se>.

BBR (2006): *BBR VT CONA CMI Bonded Post-tensioning System,* BBR, (Electronic), PDF-format, Available: <http://www.bbrnetwork.com/dowload/brochures.html>

Boverket (2004): *Boverkets handbok om betongkonstruktioner BBK 04* (Boverket´s handbook on Concrete Structures BBK 04. In Swedish), Boverket, Byggavdelningen, Karlskrona.

Broo, H., Lundgren, K. & Plos, M. (2008): *A guide to non-linear finite element modelling of shear and torsion in concrete bridges,* Department of Civil and Environmental Engineering, Chalmers University of Technology, Report 2008:18, Göteborg, Sweden, 2008.

Cederwall, K., Lorentsen, M. & Östlund, L. (1990): *Betonghandbok Konstruktion, utgåva 2* (Concrete handbook Design, 2nd edition. In Swedish), AB Svensk Byggtjänst, Solna.

CEB (1993): *CEB-FIB Model Code 1990*, Bulletin d'Information 213/214, Lausanne, Switzerland, 1993.

Cornelissen, H., Hordijk, D. & Reinhardt, H. (1986): Experimental determination of crack softening characteristics of normalweight and lightweight concrete. *HERON*, Vol. 31, No. 2, 1986, pp. 45-56.

EN 1992-1-1 (2004): *Eurocode 2, Design of concrete structures – Part 1-1: General rules and rules for buildings*, European Committee for Standardization, Brussels.

Hillerborg, A. (1985): The theoretical basis of a method to determine the fracture energy G_f of concrete. *RILEM 50-FMC*, Vol. 18, No. 106, 1985, pp. 291-296.

Jarlsson, I J (1994): *Bro 799. Inmätning av sprickor vid stöd* (Bridge 799. Mapping of cracks att supports. In Swedish), [Leaflet], SIAB, Sweden, 1994.

Johansson, K (2009): *Uppföljning kartering sprickor Axevallabron* (Follow-up of mapping of cracks in Axevalla bridge. In Swedish), [Leaflet], PEAB, Axevalla, Sweden, 2009.

Migell, R (2006): *Beträffande sprickor i ändtvärbalkar på vägport P 1415 under väg 1799 vid Hallabron* (Concerning cracks in transversal support beams on bridge P 1415 under road 1799 by Hallabron. In Swedish), [Leaflet], Inhouse Tech, Göteborg, Sweden, 2006.

Plos, M. (2000): *Finite element analyses of reinforced concrete structures,* Department of Structural Engineering, Chalmers University of Technology, Compendium 96:14, Göteborg, Sweden, 2000.

Simulia (2009a): *Abaqus 6.9 Analysis User's Manual*, Dassault Systèmes, Providence, USA, 2009.

Simulia (2009b): *Abaqus 6.9 Theory Manual*, Dassault Systèmes, Providence, USA, 2009.

Svensson, T (2009): *Kommentar till avvikelserapport Axevallabron* (Comments on deviation report Axevalla bridge. In Swedish), [Leaflet], FB Engineering AB, Sweden, 2009.

Vägverket (2005): *Minnesanteckningar från Banverkets och Vägverkets referensgrupp för dimensionering av broar* (Memory notes from Banverket's and Vägverket's reference group for design of bridges. In Swedish), [Leaflet], Vägverket, Pylonen, Borlänge, Sweden, 2005.

Vägverket (2007): *Bro 2004 – Supplement nr 2* (Bridge 2004 – Supplement no. 2. In Swedish), Vägverket, Bridge- och tunnel technology, Publication 2007:107, Borlänge.

Appendix A1 – Hand calculations of moment distribution of bridge 16-935-1

Input data

Material properties

$E_{cm} := 35GPa$ Young´s modulus for concrete

$f_{ctk0.05} := 2.5MPa$ Tensile strength of concrete

Dimensions

$b_{es} := 10.41m$ Width of integrated breast wall

$h_{es} := 2.6m + 1.359m = 3.959m$ Heigth of integrated breast wall

$l_{es} := 0.75m$ Length of integrated breast wall

$b_{tb} := 10.41m$ Width of transversal beam

$h_{tb} := 1.359m$ Heigth of transversal beam

$l_{tb1} := 1.25m$ Length of transversal beam to support 1

$l_1 := l_{es} + l_{tb1} = 2m$ Length between end of bridge and support A

$l_2 := 21m$ Length between support A and B

$l_3 := 34m$ Length between support B and C

$L := l_1 + l_2 + \frac{l_3}{2} = 40m$ Length of half the bridge

Cross-sectional areas

$A_b := 7.836445m^2$ Area of main beam

$A_{es} := b_{es} \cdot h_{es} = 41.213m^2$ Area of integrated breast wall

$A_{tb} := b_{tb} \cdot h_{tb} = 14.147m^2$ Area of transversal beam

$g := 9.82\frac{m}{s^2}$ Gravitaional accelerational constant

$\rho := 2500\frac{kg}{m^3}$ Density of reinforced concrete

Load

$q_{es} := \rho \cdot g \cdot A_{es} = 1.012 \times 10^3 \cdot \frac{kN}{m}$ Load acting on integrated breast wall

$q_{tb} := \rho \cdot g \cdot A_{tb} = 347.314\frac{kN}{m}$ Load acting on transversal beam

$q_b := \rho \cdot g \cdot A_b = 192.385 \frac{kN}{m}$ Load acting on main beam

Second moment of area

$I_{es} := \frac{b_{es} \cdot h_{es}^3}{12} = 53.83 m^4$ Second moment of area for integrated breast wall

$I_{tb} := \frac{b_{tb} \cdot h_{tb}^3}{12} = 2.177 m^4$ Second moment of area for transversal beam

$I_b := 1.28140997 m^4$ Second moment of area for main beam

Global analysis

Moment distribution

$M_A := \frac{q_{tb} \cdot l_{tb1}^2}{2} + q_{es} \cdot l_{es} \cdot \left(l_{tb1} + \frac{l_{es}}{2} \right) = 1.504 \times 10^3 \cdot kN \cdot m$ Moment at support A

$\theta_{B1} + \theta_{B2} = 0$ Continuity condition at support B

$\theta_{B1} = \frac{q_b \cdot l_2^3}{24 \cdot E_c \cdot I_b} - \frac{M_B \cdot l_2}{3 \cdot E_c \cdot I_b} - \frac{M_A \cdot l_2}{6 \cdot E_c \cdot I_b}$ Support rotation at left hand side of support B

$\theta_{B2} = \frac{q_b \cdot l_3^3}{24 \cdot E_c \cdot I_b} - \frac{M_B \cdot l_3}{3 \cdot E_c \cdot I_b} - \frac{M_C \cdot l_3}{6 \cdot E_c \cdot I_b}$ Support rotation at right hand side of support B

$M_C = M_B$ Due to symmetry

$\theta_{B2} = \frac{q_b \cdot l_3^3}{24 \cdot E_c \cdot I_b} - \frac{M_B \cdot l_3}{3 \cdot E_c \cdot I_b} - \frac{M_B \cdot l_3}{6 \cdot E_c \cdot I_b}$

$M_B := 5 kN \cdot m$ Initial guess

$M_B := root\left[\frac{q_b \cdot l_2^3}{24 \cdot E_{cm} \cdot I_b} - \frac{M_B \cdot l_2}{3 \cdot E_{cm} \cdot I_b} - \frac{M_A \cdot l_2}{6 \cdot E_{cm} \cdot I_b} + \left(\frac{q_b \cdot l_3^3}{24 \cdot E_{cm} \cdot I_b} - \frac{M_B \cdot l_3}{3 \cdot E_{cm} \cdot I_b} - \frac{M_B \cdot l_3}{6 \cdot E_{cm} \cdot I_b} \right), M_B \right]$

$M_B = 1.6\times 10^4\cdot kN\cdot m$ Moment at support B

$M_C := M_B$ Moment at support C

$x := 0, 1m .. L$ Coordinates along the bridge

$Q_{tot} := q_{es}\cdot l_{es} + q_{tb}\cdot l_{tb1} + q_b\cdot l_2 + q_b\cdot\frac{l_3}{2} = 8.504\times 10^3\cdot kN$ Load acting on the bridge

Reaction forces

$R_{A1} := q_{es}\cdot l_{es} + q_{tb}\cdot l_{tb1} = 1.193\times 10^3\cdot kN$ Reaction force at support A, left hand side

$R_{A2} := \frac{q_b\cdot l_2}{2} - \frac{M_B}{l_2} + \frac{M_A}{l_2} = 1.33\times 10^6\,N$ Reaction force at support A, right hand side

$R_A := R_{A1} + R_{A2} = 2.523\times 10^3\cdot kN$ Reaction force at support A

$R_{B1} := \frac{q_b\cdot l_2}{2} - \frac{M_A}{l_2} + \frac{M_B}{l_2} = 2.71\times 10^3\cdot kN$ Reaction force at support B, left hand side

$R_{B2} := q_b\cdot\frac{l_3}{2} - \frac{M_C}{l_3} + \frac{M_B}{l_3} = 3.271\times 10^3\cdot kN$ Reaction force at support B, right hand side

$R_B := R_{B1} + R_{B2} = 5.981\times 10^3\cdot kN$ Reaction force at support B

$R_{tot} := R_{A1} + R_{A2} + R_{B1} + R_{B2} = 8.504\times 10^3\cdot kN$ Total reaction force

Total reaction forces are the same as the total load acting on the bridge.

Moment distribution

$$M(x) := \begin{cases} \dfrac{-q_{es}\cdot x^2}{2} & \text{if } x \le l_{es} \\ \left[\left[-q_{es}\cdot l_{es}\cdot\left[\dfrac{l_{es}}{2} + (x - l_{es})\right] + \dfrac{-q_{tb}\cdot(x - l_{es})^2}{2}\right]\right] & \text{if } l_{es} < x \le l_1 \\ \left[\left[R_{A2}\cdot(x - l_1) - q_b\cdot\dfrac{(x - l_1)^2}{2}\right] - M_A\right] & \text{if } l_1 < x \le l_2 + l_1 \\ \left[\left[R_{B2}\cdot(x - l_2 - l_1) - \dfrac{q_b\cdot(x - l_2 - l_1)^2}{2}\right] - M_B\right] & \text{if } l_2 + l_1 < x \le l_1 + l_2 + \dfrac{l_3}{2} \end{cases}$$

Appendix A2 – Hand calculations of principal stresses of bridge 16-935-1

$Q_{tot} = 8.504\times 10^{3}\cdot kN$ — Total load

$l_{bear} := 5m$ — Length between bearings

$l_{load} := 4.6m$ — Assuming that the load will act on the same length as the width of the main beam

$R_{bear1} := \frac{R_A}{2} = 1.261\times 10^{3}\cdot kN$ — Assuming that the reaction force at support A from the global analysis is divide on the two bearings

$q_{sw.tb} := \frac{R_A}{l_{load}} = 548.411\frac{kN}{m}$ — Load which acts on the transversal beam

$l_0 := \frac{(l_{bear} - l_{load})}{2} = 0.2m$ — Distance from the bearing where the load is assumed to start to act

$x_{tb} := 0m, 0.1m.. \frac{l_{bear}}{2}$ — x-coordinates of half the transversal beam, defined from the middle of the left bearing.

Moment distribution along half the transversal beam:

$$M_{tb}(x_{tb}) := \begin{cases} (R_{bear1}\cdot x_{tb}) & \text{if } x_{tb} \le l_0 \\ R_{bear1}\cdot x_{tb} - q_{sw.tb}\cdot\frac{(x_{tb} - l_0)^2}{2} & \text{if } x_{tb} > l_0 \end{cases}$$

Shear force distribtution along the transversal beam:

$$V_{tb}(x_{tb}) := \begin{cases} (R_{bear1}) & \text{if } x_{tb} \le l_0 \\ R_{bear1} - q_{sw.tb}\cdot(x_{tb} - l_0) & \text{if } x_{tb} > l_0 \end{cases}$$

$I_{tb} = 2.177m^4$ — Second moment of area for transversal beam

$t_{tb} := l_{tb1} + 0.5m = 1.75m$ — Thickness of transversal beam

$h_{tb} = 1.359m$ — Height of transversal beam

$z_{GC} := \frac{h_{tb}}{2} = 0.68m$ — Center of gravity in vertical direction for the transversal beam

$z := 0m, 0.1m.. z_{GC}$

$$S(z) := t_{tb} \cdot z \cdot \left(z_{GC} - \frac{z}{2} \right)$$

First moment of area

$$\tau_{xy}\left(x_{tb}, z\right) := \frac{S(z) \cdot V_{tb}\left(x_{tb}\right)}{I_{tb} \cdot t_{tb}}$$

Shear stress along transversal beam

$$\sigma_x\left(x_{tb}, z\right) := \frac{M_{tb}\left(x_{tb}\right)}{I_{tb}} \cdot \left(z_{GC} - z\right)$$

Normal stress in x-direction along transversal beam

$$\sigma_z := 0$$

Normal stress in z-direction along transversal beam

$$\sigma_1\left(x_{tb}, z\right) := \frac{\sigma_x\left(x_{tb}, z\right) + \sigma_z}{2} + \sqrt{\left[\frac{1}{2}\left(\sigma_x\left(x_{tb}, z\right) - \sigma_z\right)\right]^2 + \tau_{xy}\left(x_{tb}, z\right)^2}$$

Max principal stress at different heights of the member

Appendix B – Input data file for STRIP STEP2 analysis of bridge 16-935-1

```
9000 STRIP-STEP2 INHOUSE   210657         169351.DAT     HÅKAN, MAX     100208
9100 BRO 16-935-1
9200 SYSTEMBERÄKNING AV SPÄNNKRAFT FÖR VERIFIERING AV FEM
2000 RAM
2010 1         35000     0.4167    1.0
2020 102  BALK N
2022 0.0            0.8171              1.359     1.281     7.8364
2022 2.0            0.8171              1.359     1.281     7.8364
2020 203  BALK N
2022 0.0            0.8171              1.359     1.281     7.8364
2022 21.0           0.8171              1.359     1.281     7.8364
2020 304  BALK N
2022 0.0            0.8171              1.359     1.281     7.8364
2022 34.0           0.8171              1.359     1.281     7.8364
2020 405  BALK N
2022 0.0            0.8171              1.359     1.281     7.8364
2022 21.0           0.8171              1.359     1.281     7.8364
2020 506  BALK N
2022 0.0            0.8171              1.359     1.281     7.8364
2022 2.0            0.8171              1.359     1.281     7.8364
2040 1         0.0         0.0                                        102  2
2040 2         2.0         0.0                          ZR
2040                                                                  203  3
2040 3         23.0        0.0                          YZR
2040                                                                  304  4
2040 4         57.0        0.0                          ZR
2040                                                                  405  5
2040 5         78.0        0.0                          ZR
2040                                                                  506  6
2040 6         80.0        0.0                                       -506 5
2050 EGEN      2    5                          UTBR           192.385   G/S
2050           1    2     0.0                  UTBR           1012      G/S
2050                      0.75                 UTBR           1012      G/S
2050           1    2     0.75                 UTBR           347.314   G/S
2050                      2.0                  UTBR           347.314   G/S
2050           5    6     0.0                  UTBR           347.314   G/S
2050                      1.25                 UTBR           347.314   G/S
2050           5    6     1.25                 UTBR           1012      G/S
2050                      2.0                  UTBR           1012      G/S
2120 0.20      0.0012              200000
2130 FSP1      MF1       1    12   18                 2230
2132 1    2    0.000     1.080                2367
2132           0.500     1.096
2132           1.000     1.095
2132           1.500     1.079
2132           2.000     1.051
2132 2    3    00.00     1.051
2132           01.00     1.003
2132           02.00     0.958
2132           03.00     0.912
2132           04.00     0.868
2132           05.00     0.828
2132           06.00     0.786
2132           07.00     0.751
2132           08.00     0.731
2132           09.00     0.724
2132           10.00     0.737
2132           11.00     0.760
2132           12.00     0.785
2132           13.00     0.816
2132           14.00     0.859
2132           15.00     0.920
2132           16.00     1.000
2132           17.00     1.085
2132           18.00     1.156
2132           19.00     1.195
2132           20.00     1.210
2132           21.00     1.214
2132 3    4    00.00     1.214
2132           01.00     1.200
2132           02.00     1.155
2132           03.00     1.083
2132           04.00     0.998
2132           05.00     0.901
2132           06.00     0.801
2132           07.00     0.708
2132           08.00     0.617
```

```
2132            09.00     0.529
2132            10.00     0.448
2132            11.00     0.374
2132            12.00     0.304
2132            13.00     0.241
2132            14.00     0.190
2132            15.00     0.150
2132            16.00     0.127
2132            17.00     0.122
2132            18.00     0.127
2132            19.00     0.150
2132            20.00     0.190
2132            21.00     0.241
2132            22.00     0.304
2132            23.00     0.374
2132            24.00     0.448
2132            25.00     0.529
2132            26.00     0.617
2132            27.00     0.708
2132            28.00     0.801
2132            29.00     0.901
2132            30.00     0.998
2132            31.00     1.083
2132            32.00     1.155
2132            33.00     1.200
2132            34.00     1.214
2132 4    5     00.00     1.214
2132            01.00     1.210
2132            02.00     1.195
2132            03.00     1.156
2132            04.00     1.085
2132            05.00     1.000
2132            06.00     0.920
2132            07.00     0.859
2132            08.00     0.816
2132            09.00     0.785
2132            10.00     0.760
2132            11.00     0.737
2132            12.00     0.724
2132            13.00     0.731
2132            14.00     0.751
2132            15.00     0.786
2132            16.00     0.828
2132            17.00     0.868
2132            18.00     0.912
2132            19.00     0.958
2132            20.00     1.003
2132            21.00     1.051
2132 5    6     00.00     1.051
2132            00.50     1.079
2132            01.00     1.095
2132            01.50     1.096
2132            02.00     1.080                2367
2130                      2    12   18                 2230
2132 1    2     00.00     0.660                2367
2132            00.50     0.714
2132            01.00     0.747
2132            01.50     0.765
2132            02.00     0.760
2132 2    3     00.00     0.760
2132            01.00     0.751
2132            02.00     0.738
2132            03.00     0.727
2132            04.00     0.716
2132            05.00     0.703
2132            06.00     0.689
2132            07.00     0.687
2132            08.00     0.700
2132            09.00     0.717
2132            10.00     0.737
2132            11.00     0.760
2132            12.00     0.785
2132            13.00     0.816
2132            14.00     0.859
2132            15.00     0.920
2132            16.00     1.000
2132            17.00     1.085
2132            18.00     1.156
2132            19.00     1.195
2132            20.00     1.210
2132            21.00     1.214
2132 3    4     00.00     1.214
2132            01.00     1.200
2132            02.00     1.155
2132            03.00     1.083
2132            04.00     0.998
2132            05.00     0.901
```

```
2132            06.00     0.801
2132            07.00     0.708
2132            08.00     0.617
2132            09.00     0.529
2132            10.00     0.448
2132            11.00     0.374
2132            12.00     0.304
2132            13.00     0.241
2132            14.00     0.190
2132            15.00     0.150
2132            16.00     0.127
2132            17.00     0.122
2132            18.00     0.127
2132            19.00     0.150
2132            20.00     0.190
2132            21.00     0.241
2132            22.00     0.304
2132            23.00     0.374
2132            24.00     0.448
2132            25.00     0.529
2132            26.00     0.617
2132            27.00     0.708
2132            28.00     0.801
2132            29.00     0.901
2132            30.00     0.998
2132            31.00     1.083
2132            32.00     1.155
2132            33.00     1.200
2132            34.00     1.214
2132 4    5     00.00     1.214
2132            01.00     1.210
2132            02.00     1.195
2132            03.00     1.156
2132            04.00     1.085
2132            05.00     1.000
2132            06.00     0.920
2132            07.00     0.859
2132            08.00     0.816
2132            09.00     0.785
2132            10.00     0.760
2132            11.00     0.737
2132            12.00     0.717
2132            13.00     0.700
2132            14.00     0.687
2132            15.00     0.689
2132            16.00     0.703
2132            17.00     0.716
2132            18.00     0.727
2132            19.00     0.738
2132            20.00     0.751
2132            21.00     0.760
2132 5    6     00.00     0.760
2132            00.50     0.765
2132            01.00     0.747
2132            01.50     0.714
2132            02.00     0.660                 2367
2140 SW              EGEN       STAND1.0
2140 FRSP-T0         FSP1       STAND1.0
2140 MF0             MF1        STAND1.0
2140 TVNG-T0         FRSP-T0    STAND1.0
2140                 MF0        STAND-1.0
2140 SW-FRSP         SW         STAND1.0
2140                 FRSP-T0    STAND1.0
2170 1    2     2                        DEF
2170 2    3     21                       DEF
2170 3    4     34                       DEF
2170 4    5     21                       DEF
2170 5    6     2                        DEF
```